LRP 611/98 June 1998

MEASUREMENT OF THE OPEN LOOP PLASMA EQUILIBRIUM RESPONSE IN TCV

A. Coutlis, I. Bandyopadhyay, J.B. Lister,
P. Vyas, R. Albanese, D.J.N. Limebeer,
F. Villone, J.P. Wainwright

Accepted for publication in
Nuclear Fusion

MEASUREMENT OF THE OPEN LOOP PLASMA EQUILIBRIUM RESPONSE IN TCV

A. COUTLIS[a], I. BANDYOPADHYAY[b], J.B. LISTER, P. VYAS, R. ALBANESE[c], D.J.N. LIMEBEER[a], F. VILLONE[d], J. P. WAINWRIGHT[a]

Centre de recherches en physique des plasmas, Association Euratom-Confédération suisse, École polytechnique fédérale de Lausanne, Lausanne, Switzerland

[a]Centre for Process Systems Engineering, Imperial College of Science, Technology and Medicine, Roderic Hill Building, London, United Kingdom

[b]Institute for Plasma Research, Bhat, Gandhinagar, India

[c]Associazione Euratom-ENEA- CREATE, DIMET, Università degli Studi di Reggio Calabria, Reggio Calabria, Italy

[d]Associazione Euratom-ENEA- CREATE, DII, Università degli Studi di Cassino, Cassino, Italy

ABSTRACT

Models of the response of the plasma current, position and shape to poloidal field coil currents have received considerable attention due to their importance in the design and predicting the performance of tokamak feedback control systems. Their increasing use has fuelled a need to validate them with experimental data. Previous attempts have always used closed loop data and whilst providing promising results were limited by the role of the feedback system.

This article presents a technique and results for the estimation of the open loop frequency response of the plasma on TCV. The results are compared with the CREATE-L model and confirm the previous good agreement with closed loop data. A simpler model has also been developed in order to understand the reasons for the good agreement and identify which plasma properties are important in determining the response. Thus an implementation of a simple circuit equation model is described and results confirming its agreement with the data are also presented. The reasons for this good agreement are discussed. An alternative modelling method combines features of both the theoretical and experimental techniques. Its advantage is that it incorporates well defined knowledge of the electromagnetic properties of the tokamak with experimental data to derive plasma related parameters. This model provides further insight into the plasma behaviour.

1. INTRODUCTION

It is important to possess an adequate model of the response of the tokamak plasma equilibrium to voltages applied to the Poloidal Field (PF) control coils, termed the plasma response model in this article. Typical parameters of interest are the variations of the plasma current, the plasma position and of the plasma contour shape, for both limited and diverted plasmas. The model should be linear, time-invariant and should describe the amplitudes and phases of the variations of the measured electromagnetic quantities as a function of the applied voltage frequency. Developing an adequate plasma response model is required for: i) simulating the behaviour of the plasma, ii) predicting the behaviour of the plasma, iii) confirming our understanding of the plasma behaviour, and ultimately, iv) improving the plasma current, position and shape feedback controller.

The importance of equilibrium response modelling for controller design is presently highlighted by the design of the ITER PF control system. On most tokamaks, controllers are low order (proportional integral derivative), based on simple plasma response models or tuned empirically. More modern control strategies exist which can optimise a cost function, take into consideration quantified model uncertainties, or perform online optimisation. All of these methods rely on a sufficiently accurate linear model of the system being available to the control engineer. Linear quadratic optimal control has been extensively studied [1, 2 and 3]. The H_∞ controller design theory has also received considerable attention [4, 5, 6] as it allows a cost function to be defined and optimised to improve performance whilst maintaining constraints which guarantee stability of the system in the presence of quantified bounds on the uncertainty of the model. Plasma shape, current and position controllers are now being designed for ITER using high order models linearised about an operating point corresponding to a particular equilibrium. The resulting controllers are tested on other models, both linear and non-linear, to ensure that the stringent ITER performance requirements can be met. Given the reliance of the ITER PF controller design on such linear models, there is a clear need to validate these models against experimental results. Given a further reliance on the newer high-order controller design methods, there is also a need to test the methodology itself in an experiment. This validation should therefore involve generating an appropriate linear model, validating the model against experiment and finally designing a controller and qualifying both the model and the method in an experiment.

There are two standard approaches to modelling and both are discussed in this article. The most prevalent method for modelling the plasma response has been phenomenological. A mathematical model is constructed from the relevant physical laws with appropriate, but often debated, simplifying assumptions. Models of the unstable vertical position response include current filament models [7] and rigid current displacement models [8]. For the plasma shape, position and current responses, the models range from simple circuit equation assumptions [9, 10, 2, 11] to high order deformable equilibrium plasma response models, such as CREATE-L [12], used in the design of the PF controller for ITER. This model accurately reproduces the closed loop behaviour of the TCV tokamak for limited discharges [13] and diverted discharges [14].

The second approach to modelling the plasma response is based on system identification. No *a priori* physics knowledge is assumed. Instead, a fit to experimental data is used to determine a suitable mathematical model. This approach has been used successfully in many fields, for example solar heating, ship steering and human speech [15]. The main features of TCV for modelling are that it is unstable with a large number of inputs (18 independently powered PF coils) and a large number of outputs (6 control parameters used in these particular experiments). These properties make TCV a challenge for such techniques. For plasma response modelling, the experimental data are collected by exciting the plasma response using suitable stimulation signals superimposed onto the PF coil demand voltages. The open loop response cannot be measured by simply opening the feedback loops, since the vertical position of the plasma is unstable once the plasma cross-section is elongated. However the open loop response can be recovered from closed loop data.

An example of earlier work is the system identification of the response of the plasma radial position of a circular plasma [16]. This identified model was compared against variations of a physics model in which the value of a coefficient was modified according to different physical assumptions. The identified model was also used to tune the gains of a proportional integral controller and is one of the earliest applications of a model to the design of a tokamak controller. Similar work on the identification of the radial position in a circular plasma and its use in tuning a proportional integral controller has been reported [17]. The plasma vertical position has received more recent attention due to the issue of its instability. The closed loop vertical position response of DIII-D was system identified and compared with a closed loop model in Ref. [18]. An open loop model of the unstable COMPASS-D vertical position response was system identified from closed loop experiments and subsequently used to develop high order controllers with improved performance [19, 20]. The system identification technique can also be used to derive linear models from non-linear simulation codes. As an example, a full multivariable linear model including the plasma current and plasma-wall gap responses was obtained from TSC code simulations of ITER [21].

In this article, we extend this previous experimental work by applying a new system identification method [22] to identify the plasma equilibrium response to all the PF coil voltages in the TCV tokamak. The experiments lead directly to an open loop model of the current, shape and position response from closed loop experiments. A model is obtained from the raw experimental data in two stages. Firstly, the amplitudes and phases of the responses are estimated for all of the input-output combinations at a pre-determined set of frequencies. The second stage is to obtain a mathematical multivariable transfer function which best fits the frequency response estimates. This has already been described in detail [23] but is not discussed further in this article.

The frequency response estimates themselves can be compared directly with open loop plasma response models. This open loop comparison corrects a recognised deficiency in previous model-experiment comparisons of the closed loop behaviour in TCV [13, 14]. A feedback system generally tends to reduce the sensitivity of the closed loop system to variations in the open loop plasma response model, whereas the success of a high-performance controller design depends on the accuracy of the open

loop model. The effect of the feedback controller is no longer present in our new open loop data and a direct comparison is possible.

The structure of the article is as follows. In Section 2, we describe the experimental techniques, the experiments performed and the analysis procedure, of which the full technical details are described elsewhere [23]. The results of the new application of this system identification procedure have proved to be extremely encouraging. The procedure leads to a surprisingly accurate model given the constraints of noise, the power supply limitations and the limited duration of the tokamak discharge flat-top. In Section 3, we present different phenomenological response models for comparison with the data. Firstly, we present the model of the response of the diagnostics in the absence of plasma, useful for benchmarking the precision of our electromagnetic model. Secondly, we introduce the CREATE-L model of the plasma response. Thirdly, in view of the success of the CREATE-L comparison, we implement a simpler circuit equation plasma response model for TCV (RZIP). Section 4 presents the detailed experimental results and compares them with these different models. The accuracy of the results can reveal differences between the assumptions made in *a priori* models. In Section 5 we develop a compromise 'Grey Box' model of the plasma, which is partly derived from a priori modelling and partly derived from experiment. This model incorporates well defined and verified *a priori* knowledge of the electromagnetic properties of the tokamak in the absence of plasma. The plasma parameters are then identified from experimental data. In Section 6, we investigate the implications of the good agreement between the experimental data, the CREATE-L model and the RZIP model. We conclude the article in Section 7. The complete experimental results and comparisons are presented in Appendix A. This article focuses on and discusses only the more illuminating comparisons.

2. EXPERIMENTAL TECHNIQUE

2.1 Introduction

TCV is a Tokamak which is ideally suited to a plasma control and modelling study as it possesses a relatively large number of independently driven poloidal field coils (Fig. 1). This feature lends an adaptability not available in most tokamaks. The coils comprise an inner set of eight E coils, an outer set of eight F coils, a single large ohmic solenoid coil (OH1) and a set of smaller ohmic coils connected in series which are all labelled OH2. The ohmic coils are primarily used for inductively driving the plasma current, while the E and F coils are mainly used for plasma shaping and positioning.

The aim of the identification procedure is to model the dynamics between the input demand voltage at the PF power supplies and the plasma electromagnetic control parameters.

2.2 TCV control system

A block diagram of the TCV Tokamak including its controller and power supply loop is shown in Fig. 2. The function of the power supply loop is to constrain the current in

the coils to follow the preprogrammed scenario as closely as the plasma control parameter feedback loop allows. We consider the power supply to be part of the open loop TCV system and thus seek to identify a model for $G(s)$ in Fig. 2. Measurements of the voltage commands to the power supplies ($\boldsymbol{u}$) and of the control parameters ($\boldsymbol{cp}$) are available.

There are five electromagnetic control parameters used in these discharges: P_VERT (the radial flux imbalance) which is a measure of radial position, TRI_OUT (the outboard field curvature) and TRI_IN (the inboard field curvature) which together define elongation and triangularity, I_p (the plasma current) and zI_p (the product of the plasma current and the vertical plasma position). Another parameter not under feedback control but considered here is Ψ_R, the difference between the R^2I_p and $R_0^2I_p$ current moments, where R_0 is the unperturbed major radius. All these parameters are estimated using linear combinations of fluxes, poloidal fields, and poloidal field coil currents. In almost all cases they are a more sensitive test of the plasma dynamics than the raw magnetic fields and fluxes, since they are generally differences between terms dominated by the plasma-less response rather than the plasma response.

A multi-input multi-output, proportional integral derivative controller, which acts through all coils, is used to stabilise the plasma position and regulate the control parameters using thyristor power supplies. Further details have been reported [24].

2.3 Coil excitation

Rather than using the E and F coils independently, they were matched symmetrically with respect to the horizontal mid-plane to form the pairs E1-E8, E2-E7, E3-E6, E4-E5, F1-F8, F2-F7, F3-F6 and F4-F5. These coil-pairs could then be driven in two modes, symmetric (where the coil-pairs receive the same voltage) and anti-symmetric (where the coil-pairs receive voltages of the same magnitude but of opposite sign).

The pairing of the coils is useful as it decouples the allowable plasma motion for plasmas which are up-down symmetric and centred on the midplane. The application of symmetric coil voltages produces no net radial field at the midplane and therefore does not drive any vertical plasma motion, while the use of anti-symmetric coil voltages produces a purely radial magnetic field on the midplane. A simple separation of the control parameters is apparent, as zI_p is the only parameter which is affected during the anti-symmetric experiments and barely affected during the symmetric experiments. Furthermore, by stimulating a pair of coils rather than a single coil, the signal-to-noise ratio of the output signal can be improved since the output response is twice as large for any given input amplitude limit. The signal-to-noise ratio of the measured input signal is also improved.

The anti-symmetric experiment set required eight separate discharges (eight coil-pairs), while the symmetric set required two more, as it included the ohmic coils. It should be noted that whereas the test signal was only applied to one coil-pair at a time, the controller used all of the inputs.

2.4 Experiment parameters

A weakly shaped plasma was chosen since no experience of this type of multivariable identification was available. A low vertical instability growth rate (~200 s^{-1}) implied a low open loop bandwidth which was considered to be more suitable for this first attempt. The main parameters were (R=0.87 m, a=0.22 m, B_ϕ=1.4 T, I_p=200 kA, κ_{95}=1.4, δ_{95}=0.23, q_a=4.6, n_e=2.2×10^{-19} m^{-3}).

During each identification experiment, measurements of the input and the output of the plant system were taken at 5 kHz, to avoid aliasing, over a time interval of 0.5 s. This is longer than the period of the lowest-frequency sinusoid. The transients following the start of the stimulation were allowed to decay for 50 ms before the experimental data was considered useful. This left 0.45 s of useful identification data for anti-symmetric stimulation. For symmetric stimulation data, the transient response of the tokamak in this configuration was found to be longer than 50 ms. The useful data was reduced to almost 0.4 s which was not sufficient to resolve the lowest frequency accurately. Any offset and linear drift was removed from the signals before analysis.

2.5 Stimulation signal

Point frequency estimates were obtained by exciting the system with a multi-sinusoidal signal. The model identification technique [23] requires a set of frequency response estimates at a predefined set of frequencies. This leads naturally to the use of a multi-sinusoidal signal to excite the system, rather than broadband excitation, because the input signal energy is concentrated at the relevant frequencies, producing more accurate estimates of the frequency response. The smoothness of the underlying response as a function of frequency is assumed.

The TCV excitation signal was designed with 29 sine waves spanning the angular frequency range 20 rad/s to 3000 rad/s. The period of the slowest sine wave in the excitation signal was designed to be 0.3 s which should have been adequately resolvable during the experiments. The highest excitation frequency was designed to be below half the sampling frequency and also above the assumed TCV bandwidth.

This excitation signal $s(t)$ injected at point s in Fig. 2 was defined by

$$s(t) = M\sum_{i=1}^{29} K_i \cos(\omega_i t + \phi_i) \tag{2.1}$$

where the phases (ϕ_i) were chosen to minimise the maximum amplitude of the total signal and the frequencies (ω_i) were defined by

$$\omega_i = 430\tan\left(\frac{\pi i}{64}\right) \tag{2.2}$$

The reasons for using this warping formula were to aid the mathematical model identification [23]. The frequencies are close enough so that resonant peaks or notches were not expected to be missed and the open loop bandwidth of the system was spanned. The weighting factor K_i was chosen to be $K_i = [1 \ \cdots \ 1 \ \ 1.4 \ \ 3 \ \ 4 \ \ 4]$ where larger weighting factors were given to the higher frequency sine waves in order to compensate for the lower gain of TCV at these frequencies

The test signal was scaled by a factor M to ensure that it was within the linear range of the power supplies but also large enough to provided sufficient signal-to-noise ratio in the resulting data. The final voltages applied to the PF coils lay within 80% of the power supply limits. This avoided power supply saturation and zero current crossing where a non-linear switch occurs in the TCV power supplies. The same excitation signal (allowing for different scaling, M) was used for all experiments. Figure 4 illustrates a stimulation signal, the raw input and output responses, and their fitted forms and residuals, during an experiment.

2.6 Frequency response estimation

If the system operates in a noise-free linear and time-invariant manner, the frequencies of the spectral components in the measured signal will match those in the test-signal exactly. The frequency spectrum of the measured signals at these frequencies is obtained by a least squares approximation.

We choose the sine and cosine of the measurement frequencies (ω_i) as basis functions and define an approximation error,

$$e_k = u(kt_s) - \sum_{i=0}^{N}\left[B_i \cos(\omega_i kt_s) + C_i \sin(\omega_i kt_s)\right] \tag{2.3}$$

where $u(kt_s)$ is the measured signal, t_s is the sampling time and $k = 1,\ldots,m$ is a time index. We compute B_i and C_i (C_0=0 if ω_0=0) such that the error $\boldsymbol{e}^T\boldsymbol{e}$ is minimised where $\boldsymbol{e}$ is the vector:

$$\boldsymbol{e} = \begin{bmatrix} e_1 & e_2 & \cdots & e_k & \cdots & e_m \end{bmatrix}^T \tag{2.4}$$

The frequency component of the measured signal at ω_i is then defined by $A_i\exp(j\phi_i)$, where $A_i = \sqrt{B_i^2 + C_i^2}$ and $\phi = \tan^{-1}(-C_i/B_i)$.

The amplitudes of the residuals (e_i) which cannot be decomposed into the measurement frequencies are a measure of data corruption due to external disturbances, measurement noise and non-linearities of the system. Therefore, the smaller the residuals, compared to the measured signals, the greater the confidence in the results of the identification procedure, Fig. 5.

The frequency spectra of all of the input and output data collected during the identification experiments is then used to obtain the open loop frequency response. To identify a 1-output, q-input system we need to have performed q experiments. For the j^{th} experiment we define the input frequency spectrum as $U_l^j(\omega_i)$ and the output frequency spectrum as $Y^j(\omega_i)$, where l indexes the inputs. An estimate of the system frequency response at each measurement frequency is given by,

$$\hat{G}(\omega_i) = \begin{bmatrix} Y^1(\omega_i) \\ \vdots \\ Y^q(\omega_i) \end{bmatrix}^T \begin{bmatrix} U_1^1(\omega_i) & \cdots & U_q^1(\omega_i) \\ \vdots & \ddots & \vdots \\ U_q^1(\omega_i) & \cdots & U_q^q(\omega_i) \end{bmatrix}^{-1} \tag{2.5}$$

The invertibility of the matrix ($\mathbf{U}_i$) at each frequency is a mild assumption that is satisfied if the corresponding matrix for the designed test-signal is invertible. If that is the case, then the experiments performed are said to be independent. One example of an independent set of experiments would be the case where the test-signal is applied to each input in turn. Applying the same stimulation signal to the symmetric and anti-symmetric coil pairs also constitutes an independent set of experiments. The condition number of the $\mathbf{U}_i$ matrices varies from 3 to 30, with lower values at higher frequencies, and so are easily invertible.

2.7 Reduction of the experimental frequency response data

The raw frequency response data can be fitted to a low order model. This was useful for the case of the anti-symmetric stimulation, for which a single low order multi-input single-output model can describe the response of zI_p to voltages applied to all coils. However, the symmetric response of the plasma is not dominated by a unique small set of modes. The model reduction procedure forces all anti-symmetric responses to have the same unstable pole, namely the vertical instability growth rate. The symmetric response of the plasma is more complex, with different modes affecting different coils. As a result, low-order multi-input single-output models relating one control parameter to all PF coils could not be obtained.

3. MODELS OF THE PLASMA RESPONSE

3.1 Introduction

We shall compare the open loop plasma equilibrium responses experimentally measured on TCV with those predicted by different plasma models. These models all generate the response of the coil, vessel and plasma currents. The linear relationship between these source currents and the diagnostic measurements of poloidal field ($\boldsymbol{B}_{\mathrm{pol}}$), poloidal flux ($\Psi$) and coil currents ($\boldsymbol{I}_{\mathrm{pol}}$) is then derived. Finally, we recreate the feedback control parameters used in the experiment, which are real-time matrix multiplications of an 'estimator' matrix onto the measurement vector [$\boldsymbol{B}_{\mathrm{pol}}$, Ψ, $\boldsymbol{I}_{\mathrm{pol}}$]. These control parameters are generally more sensitive to the choice of the plasma response model than the individual $\boldsymbol{B}_{\mathrm{pol}}$, Ψ, and $\boldsymbol{I}_{\mathrm{pol}}$ measurements, since they are mostly combinations of measurements that are dominated by the plasma-less response. All models include a power-supply model, simplified to a single-pole filter of time-constant τ_{ps}, between 0.5-0.7 ms, representing a statistical delay in the power supply response.

Firstly, we describe a 'plasma-less' model, which represents only the interactions between the applied voltages and the active currents, passive currents and diagnostic measurements. We follow with the CREATE-L linearisation of the PROTEUS non-linear code. This model can be generated for different assumptions of the conserved quantities. When comparing the models and the data, we shall see that the agreement between the experimental responses and the CREATE-L model is excellent, as could be expected from the success of our earlier closed loop response comparisons.

We have checked a simpler model, namely a fixed current distribution model. RZIP, the TCV implementation of this class of model, is described in detail. An advantage of such a simple model is that we can quantify the importance of different plasma terms and the effect of any uncertainty in their values. This type of model is suitable when many different configurations need to be assessed.

3.2 Plasma-less model

In the absence of any plasma, voltages applied to the PF coils still produce a response on the magnetic field and magnetic flux measurements and we can still define a system response from the control inputs to any output parameters. However, in this case, output signals that provide moments of the plasma current distribution should be zero. Examples are the plasma current, the vertical position of the current centroid or the radial position of the current centroid. Indeed, this property provides a sensitive test of the precision of the approximation of these contour integrals using a discrete set of field and flux sensors.

The input-output responses depend on the geometry of the tokamak, on the resistivity of the passive structures, on the resistance of the PF coils, and on the positioning of the individual diagnostic measurements. The plasma-less model therefore provides us a method of validating our electromagnetic model of the tokamak. Good agreement with the plasma-less model and poor agreement with the plasma models then implies that the model of the tokamak structure should not be the source of uncertainty. Lack of agreement would imply that our plasma model could never be correct.

The plasma-less model can be simply expressed by the circuit equations

$$\mathbf{M}_c \dot{I}_c + \Omega_c I_c = V_c \tag{3.1}$$

where the matrix $\mathbf{M}_c$ is the mutual matrix between the active PF coil currents and the passive vacuum vessel currents, grouped together as a vector of circuit currents, I_c. The vessel currents can either be taken to be filament currents or their truncated eigenmode equivalents. The diagonal matrix Ω_c is the resistance matrix of these circuits and V_c is the vector of applied voltages, zero for the passive coils.

This equation can be recast in the standard state-space representation as

$$\dot{I}_c = \mathbf{A} I_c + \mathbf{B} V_c \tag{3.2}$$

where $\mathbf{A} = -(\mathbf{M}_c)^{-1}\,\Omega_c$ and $\mathbf{B} = (\mathbf{M}_c)^{-1}$ and the state vector remains the vector of currents. In this state representation the measurable fluxes, fields and currents (the vector y) are determined by an output equation

$$y = \mathbf{C} I_c + \mathbf{D} V_c \tag{3.3}$$

where **C** represents the combination of the Green's functions and the feedback control estimator matrix and **D** = **0**. The matrices **A**, **B** and **C** therefore constitute the plasma-less model.

3.3 CREATE-L plasma response model

The CREATE-L model is a locally linearised representation of the response of a fully deformable equilibrium, derived from the PROTEUS non-linear model [25]. CREATE-L has been described in detail in [12] and is derived by linearising the equilibrium equation together with Ohm's law in the active and passive conductors as well as in the plasma itself. In this model, the plasma is assumed to be in permanent MHD equilibrium and the plasma current density profile is kept fixed, whereas the total plasma current is allowed to vary. The boundary and magnetic axis fluxes are also allowed to vary.

The dynamic evolution of the currents flowing in all the conductors, including the PF coils, the passive conductors, and the plasma, is described by:

$$\mathrm{d}\Psi/\mathrm{d}t + \Omega I = V \tag{3.4}$$

where Ψ is the vector of fluxes linked with each conductor and Ω is the resistance matrix. I and V are the conductor currents and applied voltages respectively. Expanding the currents $I(t)$ about their reference values:

$$I(t) = I_{\mathrm{ref}} + \delta I(t) \tag{3.5}$$

it is possible to obtain the linearised form of (3.4):

$$\mathbf{L}^{*}\,\mathrm{d}(\delta I)/\mathrm{d}t + \Omega\,\delta I = \delta V \tag{3.6}$$

where V is the coil voltage vector which is zero for the passive circuits and $\mathbf{L}^{*} = \partial\Psi/\partial I$ is the modified inductance matrix. The latter is obtained by solving a linearized form of the free boundary equilibrium problem after meshing the area of interest and assuming a given equilibrium [12]. The model is completed by the response to l_{i} and β_{p} variations. However, we are only interested to the plasma response to the conductor currents in the present work, and therefore neglect these terms.

As before, the circuit equations are conveniently cast in a state space form:

$$\mathrm{d}x/\mathrm{d}t = \mathbf{A}\,x + \mathbf{B}\,u \tag{3.7}$$

where $\mathbf{A}=-\mathbf{L}^{*-1}\Omega$, $\mathbf{B}=\mathbf{L}^{*-1}$, the currents constitute the state vector, $x = \delta I$, and the voltage input is the control vector, $u = \delta V$. The output variables of interest are the perturbations of fluxes and fields measured by magnetic sensors, and current moments. They are linear combinations of state variables as before.

All of the CREATE-L models used up to date exclude the presence of skin currents at the plasma boundary, and assume zero plasma resistivity. An alternative model has

also been derived with the additional constraint that the poloidal flux be frozen at the plasma boundary. Previous work had shown that the nominal model is in good agreement with TCV closed loop experiments, but that the frozen flux model had been invalidated [14], but we repeat this comparison for interest.

3.4 Constant current distribution model - RZIP

We describe the development of a simpler model than the CREATE-L linearised equilibrium model. We construct a set of circuit equations based on the supposition that the plasma current distribution remains constant during any control action, but that its centroid can move vertically and radially and its integral, the total plasma current, can change. The model is inherently linear and is similar to the RCDM model developed previously for the modelling of only the vertical plasma motion of vertically unstable TCV plasmas [7, 18, 8]. This model has now been extended to include control actions that modify the poloidal flux, along the lines of previous work [9, 10, 2, 11]. The main advantages of a simpler model are that it requires less effort to construct, does not necessarily need a plasma equilibrium and is more explicit in the quantities that define the plasma response.

The RZIP (R, z, I_p) plasma model is based on the linearisation assumption that small variations in the PF coil voltages lead to small changes in the plasma current, PF currents, vacuum vessel currents and the plasma radial and vertical positions. These small variations occur about a given unperturbed equilibrium state. It is assumed that the equilibrium parameter $\Lambda \equiv \beta_p + l_i / 2$ remains fixed, although variations in this parameter can be introduced as a disturbance, as in the case of the CREATE-L model.

The equations defining the structure are firstly the circuit equations for the PF coils and the vessel currents, as for the plasma-less model. In addition, we add the time derivatives of the radial and vertical force balance equations and the poloidal flux conservation equation. In these equations, notations such as A_R' and A_z' represent the derivatives of quantity A with respect to the radial (R) and vertical (z) co-ordinates respectively. Those quantities that are dependent on the plasma current distribution, namely the convolution integrals of magnetic fluxes and fields as well as their radial and vertical position derivatives, are obtained by averaging over the plasma current distribution derived by the TCV LIUQE equilibrium reconstruction code [26]

$$\langle A \rangle = \frac{\sum_i A(r_i, z_i) \cdot J_{\text{tor}}(r_i, z_i)}{\sum_i J_{\text{tor}}(r_i, z_i)} \tag{3.8}$$

where A is any of the parameters of interest.

The PF coil and vessel current circuit equations are based on calculating the flux derivative for each circuit, including the new plasma current terms, and become

$$\mathbf{M}_c \dot{\boldsymbol{I}}_c + \left(\boldsymbol{M}_R'\right)^T I_p \dot{R} + \left(\boldsymbol{M}_z'\right)^T \dot{z} I_p + \boldsymbol{M}_p{}^T \dot{I}_p + \boldsymbol{\Omega}_c \boldsymbol{I}_c = \boldsymbol{V}_c \tag{3.9}$$

where $\boldsymbol{M}_R$, $\boldsymbol{M}_z$, and $\boldsymbol{M}_\mathrm{p}$ are row vectors and the subscript 'p' refers to the mutual inductances with respect to the plasma current. We choose the eigenmode representation for the passive vessel currents.

The vertical force balance equation, ignoring the plasma mass as in previous work, remains

$$\boldsymbol{M}_z'\boldsymbol{I}_\mathrm{c} - \alpha\cdot(zI_\mathrm{p}) = 0 \tag{3.10}$$

where $\alpha = -(2\pi R_0/I_{\mathrm{p}0})(\partial B_R/\partial z)_{z=z0}$. Due to the lack of any dynamics in the vertical force balance equation, the zI_p state variable could be eliminated, however it is retained in what follows to clarify the development of the model.

The perturbed radial force balance equation is expressed by the time derivative of its linearised variation

$$\frac{d}{dt}\left[\delta\sum F_R\right] = 0 = \frac{\mathrm{d}}{\mathrm{d}t}\left[\delta\left\{2\pi R I_\mathrm{p}\left(B_\mathrm{hoop}(R) + B_\mathrm{ext}(R)\right)\right\}\right] \tag{3.11}$$

which implies

$$\boldsymbol{M}_R' I_{\mathrm{p}0}\dot{\boldsymbol{I}}_\mathrm{c} + \left[\frac{\mu_0 I_{\mathrm{p}0}^2}{2}\frac{\partial\Gamma}{\partial R} + 2\pi I_{\mathrm{p}0}B_{z0} + 2\pi R_0 I_{\mathrm{p}0}B_{z0}'\right]\dot{R} + \left[\mu_0 I_{\mathrm{p}0}\Gamma_0 + 2\pi R_0 B_{z0}\right]\dot{I}_\mathrm{p} = -\frac{\mu_0 I_{\mathrm{p}0}^2}{2}\dot{\Gamma} \tag{3.12}$$

where the Shafranov parameter is taken to be $\Gamma = \ln\left(\frac{8R_0}{a\sqrt{\kappa}}\right) + \Lambda - \frac{3}{2}$.

The perturbed flux conservation equation becomes

$$\boldsymbol{M}_\mathrm{p}\dot{\boldsymbol{I}}_\mathrm{c} + \left[\mu_0(1+f_0)I_{\mathrm{p}0} + 2\pi R_0 B_{z0}\right]\dot{R} + L_{\mathrm{p}0}\dot{I}_\mathrm{P} + I_{\mathrm{p}0}\Omega_\mathrm{p}' R + \Omega_\mathrm{p} I_\mathrm{p} = 0 \tag{3.13}$$

where Ω_p is the plasma resistance, $f_0 = \ln\left(\frac{8R_0}{a\sqrt{\kappa}}\right) + \frac{l_\mathrm{i}}{2} - 2$ and $L_{\mathrm{p}0} = \mu_0 R_0 f_0$ is the plasma inductance. This equation can also be eliminated as a combination of modified states, but as before we retain it for clarity.

These equations (3.9-3.12), with some abuse of notation, can be combined as follows:

$$\begin{bmatrix} \mathbf{M}_\mathrm{c} & \left(\boldsymbol{M}_z'\right)^\mathrm{T} & \left(\boldsymbol{M}_R'\right)^\mathrm{T} & \left(\boldsymbol{M}_\mathrm{p}\right)^\mathrm{T} \\ \boldsymbol{M}_z' & \alpha & 0 & 0 \\ \boldsymbol{M}_R' & 0 & M_{33} & M_{34} \\ \boldsymbol{M}_\mathrm{p} & 0 & M_{43} & L_{\mathrm{p}0} \end{bmatrix} s \begin{bmatrix} \boldsymbol{I}_\mathrm{c} \\ zI_{\mathrm{p}0} \\ RI_{\mathrm{p}0} \\ I_\mathrm{P} \end{bmatrix} + \begin{bmatrix} \Omega_c & 0 & 0 & 0 \\ 0 & 0 & 0 & 0 \\ 0 & 0 & 0 & 0 \\ 0 & 0 & \Omega_\mathrm{p}' & \Omega_\mathrm{p} \end{bmatrix} \begin{bmatrix} \boldsymbol{I}_\mathrm{c} \\ zI_{\mathrm{p}0} \\ RI_{\mathrm{p}0} \\ I_\mathrm{P} \end{bmatrix} = \begin{bmatrix} \boldsymbol{V}_\mathrm{c} \\ 0 \\ -\frac{\mu_0 I_{\mathrm{p}0}^2}{2} s\Gamma \\ 0 \end{bmatrix} \tag{3.14}$$

where s is the Laplace variable, the states have become functions of s and where

$$
\begin{aligned}
M_{33} &= \left[\frac{\mu_0}{2} \frac{\partial \Gamma}{\partial R} + \frac{2\pi}{I_{p0}} \left(B_{z_0} + R_0 \frac{\partial B_z}{\partial R} \right) \right] \\
M_{34} &= \mu_0 \Gamma_0 + 2\pi R_0 B_{z_0} / I_{p_0} \\
M_{43} &= \mu_0 (1 + f_0) + 2\pi R_0 B_{z_0} / I_{p0}
\end{aligned}
\tag{3.15}
$$

In the nominal RZIP model, we assume that $d\Gamma/dR = 1/R_0$, $\Omega_p' = 0$, $\Omega_p = 0$. These simplifying assumptions will be investigated when examining the results.

This equation can be re-expressed in the standard state-space form as before. The structure of this equation is similar to that of Eq. (3.1) of the plasma-less model. The change of the R and I_p responses due to the presence of the plasma is restricted to the coefficients M_{33}, M_{34}, M_{43}, L_{p0}, Ω_p and Ω_p'. As in the case of the vertical position, the radial position component of Eq. (3.14) has no dynamics and could be re-expressed as an output equation. This corresponds to the radial equilibrium being instantaneously satisfied. Any variation of the Shafranov parameter Γ appears as its time derivative in the third row of the equation. Time-variations of β_p and l_i are therefore treated, although this feature is not discussed further in this article.

The driving terms of the plasma equations are the integrals of the field gradients over the plasma current cross section. In the nominal RZIP model, these are calculated by integrating over the reconstructed equilibrium current profiles, known after the discharge and are useful for *a posteriori* comparisons. We have also investigated two even simpler assumptions, namely that the current distribution be approximated by a circular or elliptical cross section with a parabolic profile, $j(r) = (1\text{-}r^2/a^2)$, referred to as the RZIP-0 models. These have the advantage of not being dependent on reconstructed current profiles and can be evaluated before a discharge.

4. RESULTS

4.1 Introduction

In this section, we present the experimental results and compare them with the different models described. In view of the quantity of information generated by such experiments, we present only a representative selection in this article. A complete set of the graphical data has been presented in Appendix A. It is possible to consider each coil voltage as an individual input, as derived in the models. However we have chosen to retain the symmetric and anti-symmetric combinations as inputs as used in the experiments. We subsequently present the data in a 'decoupled' form, making a new set of up-down symmetric inputs that drive essentially the radial position, the plasma current and the plasma elongation.

4.2 Plasma-less experiments

The vacuum vessel and PF system model was validated with a series of tests on the TCV tokamak with no plasma. The feedback loop for the control parameters was opened and the same multi-sinusoidal excitation signal as defined above was applied

to the input of each power supply in turn. In these experiments only a single coil was driven at any time. Following the procedure described in Section 2, a least squares fit was used to find the frequency components in the input and output signals. Then the system frequency response was obtained by collating all the frequency point estimates and inverting as in Equation (2.5). The output variables examined included all the diagnostic poloidal fields and fluxes, the PF coil currents and the control parameters. Where the variance of the estimates is low the model-estimate fit is extremely accurate. Typical errors lie within 1 dB and 5 degrees for frequencies below 1000 rad/s (Fig. 3). When the output amplitude responses are small, the signal to noise and hence the estimate variance is inevitably poorer but the data from all coil inputs to all control parameter outputs never invalidate the model.

4.3 Unstable Vertical Plasma Movement

Only the zI_p control parameter is modelled for the anti-symmetric stimulation. The experimental data from the anti-symmetric coil-pair experiments were processed as described in Section 2 to generate the frequency responses. These data were then further analysed to produce separate impulse responses of the stable and unstable parts of the system [23]. The order of these models was then examined showing that the unstable system was dominated by a single pole, while the stable part could be approximated by a 3-pole model. As expected, the single unstable mode corresponds to the existence of the plasma vertical instability.

The reduced 4th order model is numerically described by

$$zI_p(s) = [\text{E18 E27 E36 E45 F18 F27 F36 F45}]\times \frac{\begin{bmatrix}1.92\times10^{-5}\\2.85\times10^{-5}\\2.17\times10^{-4}\\2.75\times10^{-4}\\1.75\times10^{-7}\\8.10\times10^{-6}\\5.05\times10^{-5}\\1.31\times10^{-5}\end{bmatrix}s^2+\begin{bmatrix}5.99\times10^{-2}\\1.83\times10^{-1}\\4.89\times10^{-1}\\3.18\times10^{-1}\\-1.01\times10^{-3}\\6.22\times10^{-2}\\1.96\times10^{-1}\\1.37\times10^{-1}\end{bmatrix}s+\begin{bmatrix}39.6\\46.8\\66.6\\35.9\\21.0\\26.1\\32.8\\18.7\end{bmatrix}}{-2.43\times10^{-11}s^4-6.2\times10^{-8}s^3-2.85\times10^{-5}s^2+4.42\times10^{-3}s+1} \quad (4.1)$$

with the addition of a time delay of 0.7 ms which represents delays due to the power supplies. Here E18 is shorthand for the voltage demand signal to the E1 and E8 power supplies in anti-symmetric stimulation.

This identified model was compared with the RZIP and CREATE-L models, Fig. 6. The models are all in excellent agreement. The amplitude plots show that the model-experiment difference is of the same order as the variance of the experiment estimates. Even though the responses span a very large dynamic range, over 50 dB, the agreement is still good. This is especially remarkable at high frequencies with very low gains. The largest level of disagreement occurs below 5 rad/s for the coils F3+F8

where the disagreement is less than 2 dB and coils E2+E7 where the disagreement is consistently approximately 3 dB. The phase response agreement is always within the variance of the estimates except above 500 rad/s for coils F1+F8. The typical level of difference is less than 5 degrees.

The predictions of the growth rate of the vertical instability are very close (213 s^{-1} identified compared with 209 s^{-1} for the RCDM). This is an encouraging validation of the consistency of the identified and the physics based models. The identified model can also be used to look for discrepancies in the physics based model and in Fig. 6 we can see room for improvement in the amplitude response of the E2-E7 coil-pair.

4.4 Flux-varying responses

The same comparisons of the input-output transfer functions have been made for the symmetric responses. The agreement is generally excellent, as illustrated by Fig. 7 in which a sample of the responses is shown. Transfer functions can be contructed using this experimental data [23] but this is not described here.

The apparent variance of the experimental frequency response estimates varies according to the choice of input-output pair. However for each pair it remains roughly constant in dB units across the range of frequencies. When the variance is low, the agreement between the models and the data is generally good and there is normally no variation between the models. The phases rotate smoothly as frequency increases. At the highest frequencies, the response gain is usually small and the amplitude and phase become more uncertain. There are too few cycles of the lowest frequency stimulation to obtain an accurate measurement and these data show a regularly large departure from a smooth frequency dependence. Thus the lowest frequency data have been disregarded.

In general we find that both the RZIP model and the CREATE-L models agree with the experimental estimates to within the variance of the estimates (41 cases out of 50). A typical case is F3+F6 to Ψ_R, (Fig. 7a) which has frequency estimates with a variance of approximately 1 to 2 dB in the amplitude response and less than 5° in the phase response. The plasma models agree both with each other and with the experimental data. The plasma-less model has a much smaller amplitude response indicating that the plasma is a very sensitive component of the model. The plasma model agreement in this case can be considered with confidence as an indicator of the quality of the models.

Occasionally we find transfer functions in which the plasma-less response also agrees well with the data (Fig. 7b). In all these cases the plasma models have an almost identical response to the plasma-less model (8 of the TRI_IN and TRI_OUT responses). The plasma plays little or no part in the response and so the plasma model assumptions make no difference to the plasma response. It is not surprising that the agreement between the models and experiments are then so good, because we know from vacuum tests that the electromagnetic properties of TCV are well modelled. For this reason we consider the use of plasma current moments, such as Ψ_R, to be a more suitable test of the physics assumptions, although the use of flux control parameters

would be sufficient if it is only the validity of the model for control design which is being tested.

In some rare cases clear differences between the RZIP model and the CREATE-L model can be observed. These cases are not specific to either the stimulation or the response parameter except for a trend of large variances with E2+E7 stimulation. In principle the experimental data could be used to distinguish the model with the correct assumptions. In practice the variance of the estimates are too poor to resolve the model differences. This tends to suggest a link between the estimate variances and the sensitivity of the modelled responses to the physics assumptions. This could be due to a number of reasons. One possibility is a nonlinear response which can only be poorly linearized by a model and which is difficult to measure by linear frequency transform methods. Another possibility is that the effect of plasma disturbances become dominant in these particularly sensitive transfer functions. However neither of these possibilities have been confirmed.

The difference between physics models for E2+E7 responses can be understood in terms of the properties of the vacuum field created by the particular stimulation. Figure 8 illustrates the vertical field and total poloidal flux modifications when the coil currents are changed. E2 and E7 are placed at the poloidal location where the vertical field created by a coil current crosses zero, displaced inwards by the toroidicity. At the same place, the DC contribution of these coil currents to the net poloidal flux is also small. The direct influence of these coils is therefore exceptionally small and the response becomes very sensitive to small differences in the models. However, these coils have a large coupling to elongation or triangularity and the experimental response from E2+E7 to TRI_IN has an excellent signal-to-noise ratio.

An unusual case (Fig. 7c) shows the experimental response lying clearly between the RZIP and CREATE-L responses. For the response of I_p to stimulation from coils E4 and E5 we cannot determine which model is the closest. These discrepancies only occur for some of the I_p and Ψ_R responses. This was not previously seen in closed loop responses [13] and highlights the role of the feedback system in reducing the sensitivity of the performance of the closed loop system to changes in the response of the open loop system.

4.5 Decoupling of the stimulation

At first sight, it is surprising that the RZIP model, which has primitive assumptions, should show as good agreement with the experimental data as CREATE-L which was developed from a deformable equilibrium model. The most significant term that is lacking in the RZIP model is the deformation of the plasma current distribution itself. We consider the changes to the poloidal field structure imposed by the active and passive currents as being decomposable into independent quantities. These were evaluated by integrating them over the reconstructed current profile. The first is the radial field, which drives the vertical position. The second is the vertical field that predominantly determines the radial position. The third is the poloidal flux that predominantly determines the plasma current. The fourth is the quadrupole field that determines α, the coefficient that affects the vertical position instablity growth rate.

To first order, the first three have no effect on the plasma current profile. The quadrupole field is the first moment which deforms the profile, followed by the hexapole field. This simple decomposition should provide an insight into whether the relevant responses are correctly modelled. We might suppose that the reaction to a quadrupole field change would be the first plasma response that is incorrectly modelled. We verified that the effect of the coil voltage pattern generating a purely quadrupole field at low frequency indeed modified the elongation more that parameters, seen from the reconstructed equilibria.

There is no change in the quality of the agreement between the application of the fields included in the model and other fields not included in the model. For example Fig. 9 illustrates the RZIP, CREATE-L and experimental responses to the quadrupole field. This implies that the deformation of the current profile caused by the quadrupole field has a much smaller effect on the control parameters than the deformation of the vacuum field itself.

5. GREY BOX MODEL

5.1 Introduction

The results have illustrated that both the CREATE-L and the RZIP models agree with the experimentally identified frequency estimates. It is also possible to develop a model solely from these frequency point estimates [23]. The advantage of such a system identified model is that no *a priori* information is required about the plasma response. Here we developed a hybrid approach to modelling which incorporates well defined *a priori* knowledge for part of the model, and experimental data is used to identify the parts of the plasma response which are more susceptible to error. The generally used term for this approach is 'Grey Box modelling' and is used to contrast 'White Box Modelling' which refers to a model based purely on *a priori* knowledge and 'Black Box Modelling' which refers to a parameterised model based purely on experimentally acquired information. Grey Box modelling is particularly suited to our present problem due to the large number of known coefficients compared with the small number of uncertain coefficients. Later, we compare the resulting 'Grey Box Model' with the *a priori* models and with the experimental data.

5.1 Grey Box development

In the circuit equations (3.9-3.13), we find a large number of coefficients. These are condensed into the reduced form (3.14). In this representation, the inductance matrix $\mathbf{M}_c$ is the inductance between the active coils and the passive vessel currents. The resistance matrix is diagonal for all the circuits that have no interconnections and contains the simple circuit resistances. All of these coefficients are independent of the presence of the plasma and can, in principle, be modelled or measured with unlimited precision given the required effort. They are therefore knowable *a priori*. Experiments carried out in the absence of plasma can test the validity of these parts of the complete circuit equations (Section 4.2). Since these matrix elements constitute most of the non-zero matrix elements in the full circuit equations, we already see that the 'Grey'

part of the model is a very small fraction of the total model. The model is divisible into 'Black' and 'White' parts in the frame of the circuit equations, and not in the frame of the standard state space form.

The plasma-related parts of the circuit equations are $\boldsymbol{M}_R'$, $\boldsymbol{M}_z'$, α, $\boldsymbol{M}_p$, M_{33}, M_{34}, M_{43}, L_{p0}, Ω_p and Ω'_p . The terms $\boldsymbol{M}_R'$, $\boldsymbol{M}_z'$, α, and $\boldsymbol{M}_p$ are integrals over the plasma current distribution which are only very slightly dependent on the plasma current distribution, as we have deduced and as we shall demonstrate later. This is a corollary of the difficulty of measuring the plasma current distribution from magnetic measurements made outside the plasma volume. We have reason to believe that these elements are then adequately determined by our *a priori* knowledge and we include them in the 'White' part of the model.

Our GBM is therefore defined by the coefficients M_{33}, M_{34}, M_{43}, L_{p0}, Ω_p and Ω'_p. The GBM is therefore determined by six unknowns and each point in $\mathbf{R}^6$ is a particular instance of a candidate GBM. The 'White Box Model' of Section 3.4 is a particular GBM. Each GBM will produce an open loop plasma response of the control parameters to the coil voltage inputs, as a function of frequency. We therefore evaluate the 10×5 input-output transfer functions for up-down symmetric connections of the coil inputs and up-down symmetric responses at each of the 28 frequencies.

In order to choose between the possible GBMs we need to define a cost function to measure the agreement between the experimental data and the GBM. A search on the GBM parameters minimising the function produces the 'Best GBM' (BGBM). Note however that this BGBM will be dependent on the form chosen for the cost function and so the function should be chosen carefully. The large variation in the magnitudes of possible responses, the apparent constant variance on a logarithmic scale and the possible increases in the experimental estimate variance at low and high frequency and for small gains, combined with the amplitude and phase of the model to be fitted, led us to test several cost functions, to find one which corresponded to our visual appreciation of the fit. We have chosen to use a simple relative error comparing the system identified response G_{SI} with the GBM response G_{GBM}

$$Q = \sum_{cp} \frac{\sum_i \sum_\omega \left| G_{SI}(cp,i,\omega) - G_{GBM}(cp,i,\omega) \right|}{\left\langle \left| G_{SI}(cp,i,\omega) \right| \right\rangle} \tag{5.1}$$

where the sums are over frequencies ω, inputs i, and control parameters cp. The absolute value of the model error is used rather than its square to reduce the importance of outliers. There is a weighting on each control parameter (the denominator) because they have different dimensions. The frequencies are weighted uniformly. The minimum of the cost function is found by allowing a number of parameters to be varied by a standard simplex minimisation procedure.

5.3 Modelling results

The BGBM was found by setting all six Grey parameters to zero and searching first for the optimal four elements of the mutual matrix. Once a minimum was found, the

two resistance values were also floated and both these parameters were optimised. Finally, all six elements were freed to find a global optimum. This approach is 'unbiased' in the narrow sense that the search does not begin with the 'White' *a priori* values of these parameters. Having found the BGBM, a single parameter scan was performed on each adjusted element, over a range 0-4 times the values of the BGBM parameters. The results of this scan are shown in Fig. 10. The parameter causing the most rapid variation of the cost function is L_{p0}, the plasma inductance. The next sensitive paramefer is M_{33}, which defines the Shafranov equilibrium constraint. The parameters M_{34} and M_{43} have much shallower minima and predominantly define the interactions between the loop voltage and the position and between the vertical field and the plasma current. Finally, the resistive terms, Ω_p and Ω_p', are the most shallow.

The vertical lines show the values of the *a priori* model parameters. The value of L_{p0} is the most sensitive and is measured to be within a few percent of the *a priori* value. The BGBM value of M_{33} is 50% greater than the *a priori* value. M_{34} and M_{43} are 15-25% of their *a priori* values, but this does not significantly change the quality of the fit. The resistance Ω_p is 20 μΩ, compared with 5.4 μΩ for the DC plasma column resistance. It is reasonable that the BGBM value should be greater than the DC value, since any plasma current variation is not homogeneous over the plasma cross section, but concentrated towards the edge in a smaller area of a cooler plasma. In order to identify the plasma resistance with more precision, lower frequency stimulation would be required. The value of $\Omega_p' I_p$ is found to be –10.0 V/m for the BGBM. The predicted value is

$$\Omega_p' I_p = \Omega_p I_p (1/R - 2/a) = -7.7 \text{ V/m} \qquad (5.2)$$

in which we assume that the resistance simply varies with the length and cross-sectional area of the plasma. This negative value corresponds to the particular case of a plasma limited on its inboard side. Assuming that Ω_p and Ω_p' are both equal to zero does not lead to a significant error in the model.

The *a priori* model produced a GBM cost function value of 536, whereas the BGBM resulted in a cost function value of 378. Without varying Ω_p and Ω_p' the value of the cost function is 405. The difference is relatively small and we should therefore not expect the transfer functions to be extremely different from the *a priori* transfer functions. Fig. 7 shows BGBM transfer functions superimposed on the *a priori* transfer functions. Most are unchanged to the eye, but a visible improvement occurs in 5 out of the 50 input-output relationships. The cases with the worst *a priori* model fit have been significantly rectified, as illustrated in Fig. 7c. Apart from an overall slight improvement, the plasma current response has shown the most significant improvement. This is not due to a modification of the apparent plasma inductance, as expected, but has been obtained from the Shafranov equation terms. In this way, the E4+E5 to I_p transfer function has been increased to close to its measured value without having modified all of the I_p transfer functions, which would have been the case with a straightforward modification to L_p.

Having located the BGBM, we floated the power supply time-constant, τ_{ps}, finding a minimum at 0.6 ms, Fig. 11, compared with the average thryistor firing delay of 0.6

ms, confirming the value of 0.7 ms found previously in closed loop tests by trial and error. Finally, we floated the number of eigenmodes required for the description of the vacuum vessel current distribution, also shown in Fig. 11. The cost function drops in a step-wise fashion, as the most significant eigenmodes are included, dropping to close to the minimum once 15 eigenmodes are included. The order of the RZIP model with 15 eigenmodes is 15 (for the vessel) + 18 (for the coils) + 1 (for I_p) = 34. Certain eigenmodes could be neglected by inspection, but this would be neither general nor efficient.

We conclude this section summarising what we have learned from the Grey Box modelling:

- the BGBM has only a slightly better fit to the data than the nominal RZIP model
- the values of the nominal RZIP model have been determined absolutely using the GBM technique, validating them positively from no *a priori* assumptions
- the parameters which have a strong effect on the comparison with the data have been identified and agree with the nominal model
- the parameters which have a weak effect have been identified and the nominal model is close to the BGBM
- the most suitable power supply model is also defined by this procedure
- a suitable number of eigenmodes for the model is defined by this procedure
- the GBM technique has shown that the System Identification results contain information which allows us to determine the plasma part of the defining circuit equations.

6. DISCUSSION

The discharges analysed in this article have a relatively weak elongation, $\kappa = 1.4$. We have investigated whether the good agreement found is limited to this low elongation and how sensitive the model is to changes in the equilibrium. Firstly we derive the RZIP model for more strongly shaped TCV plasmas, not yet analysed by the system identification techniques, in the range $1.18 < \kappa < 1.82$, and $-0.2 < \delta < 0.35$. Figure 12 shows the extreme cases of elongation and triangularity and Table TABEXTREQUIL details the four dynamic variables in the mutual matrix. The parameters which were found to be most important have a small range over these equilibria, whereas the parameters which vary the most in Table TABEXTREQUIL are those with the least effect on the model. The model therefore ought to be relatively insensitive to these differences, except for the zI_p response. Figure 13 confirms this for selected input-output pairs. The case F1+F8 to P_VERT is chosen to illustrate an almost total independence on the equilibrium and E2+E7 to TRI_IN is the most dependent case. We conclude that the response is remarkably insensitive to the equilibrium current distribution. Note that the response is dependent on the vertical and radial position of the plasma axis. However this is of less concern because the plasma magnetic axis is more easily measured and controlled than the current profile.

In order to test this further we derived two even simpler models (RZIP-0), one based on an assumed circular plasma current distribution and the other based on an with elliptical distribution of the outer magnetic surface (Fig. 14). Both have a parabolic

radial profile. Figure 15 confirms the insensitivity to the details of the current profile to this extreme extent. The main reason for this is that the integrals over the current profile cancel out the modifications to the current profiles. However, we should be careful not to over-interpret this finding. We have ascertained that the linearised responses of the linearly combined diagnostic measurements to the coil voltages are relatively insensitive to the current distribution. The plasma equilibrium itself is of course extremely sensitive to the current profile and we should avoid concluding that the response of the separatrix is independent of the current profile, since integrating the linearised response cannot lead to the non-linear behaviour of the equilibrium itself. Our conclusions must be limited to the linearised response. However, it is the linearised response which determines whether we can develop a feedback controller for rejecting plasma disturbances, or for recovering from offsets in the plasma shape. The overall separatrix location will have to be derived from a non-linear inverse equilibrium code, or pre-defined by programmed PF coil currents. The inverse equilibrium code presents a nonlinear static map between the diagnostic measurements and the plasma shape and does not contribute to the dynamical part of the tokamak model.

7. CONCLUSION

In this work we have demonstrated a direct measurement of the open loop response of the multi-input multi-output unstable tokamak system, while operating in closed loop, using a new technique applied for the first time to such a large scale unstable plant. We have achieved a signal-to-noise level which is adequate for comparing models, in spite of the real experimental conditions of a noisy tokamak installation and a restricted pulse length. The resulting precision is considerably better than expected.

The experimental results for the unstable vertical movement and growth rate compare well with both the simple RCDM and CREATE-L models.

For perturbations which include poloidal flux variations leading to plasma current, shape and radial position variations, the experimental results also compare well with the CREATE-L model. We have implemented RZIP, a circuit equation plasma response model, and the experimental results also compare well with RZIP for these perturbations.

The simplicity of the RZIP model allowed the development of a 'Grey Box' model of the equilibrium response, assuming complete knowledge of the electromagnetic properties of the vacuum electromagnetics and letting the 'physics' variables be fitted from the available data. The sensitivity of the cost function indicates which physics parameters are important for good model agreement and which are not, and confirms that the *a priori* RZIP model provides a good description of those parameters which are important for the accuracy of the model.

The RZIP model was applied to extreme shapes of κ and δ scans, demonstrating that the model is relatively insensitive to shape changes. An even simpler model, based on a simplified current profile, gives virtually indistinguishable results, allowing it to be

used before the tokamak discharge has been produced. This insensitivity provides some reasons for the good agreement of the model. This suggests that the simple RZIP model would be a useful tool for the design of robustly stabilising controllers. Validating these conclusions at higher elongation and higher triangularity will be the object of future work.

ACKNOWLEDGEMENTS

It is a pleasure to acknowledge the technical support of the TCV team. Encouragement by the Naka ITER JCT is welcomed. This work was partly supported by Euratom mobility contracts (FV [ENEA] and AC [UKAEA]) and partly by the Fonds national suisse de la recherche scientifique.

REFERENCES

[1] OGATA, A., NINOMIYA, H., Proc. 8th Symp. Engineering Problems of Fusion Research, San Francisco, USA, November 1979 **4** (1979) 1879

[2] KESSEL, C.E., FIRESTONE, M.A., CONN, R.W., Fusion Techol. **17** (1990) 391.

[3] PORTONE, A., et al., Fusion Technol. **32** (1997) 374

[4] AL-HUSARI, M.M.M., et al., Proc. 30th IEEE Conf. Decision and Control, Brighton, England, December 1991 (1991) 1165-1170.

[5] PORTONE, A., PhD Thesis, University of London, Imperial College of Science, Technology and Medicine, 1994.

[6] AMBROSINO, G., et al., Proc. 36th IEEE Conf. Decision and Control, San Diego, USA, December 1997 (1997) 3697.

[7] LAZARUS, E.A., LISTER, J.B., NEILSON, G.H., Nucl. Fusion **30** (1990) 111.

[8] LISTER, J.B., MARTIN, Y., MORET, J.-M., Nucl. Fusion **36** (1996) 1547.

[9] NEILSON, G.H., DYER, G.R., EDMONDS, P.H., Nucl. Fusion **24** (1984) 1291.

[10] LAZARUS, E.A., NEILSON, G.H., Nucl. Fusion **27** (1987) 383.

[11] WAINWRIGHT, J.P., COPSEY, D.R., LIMEBEER, D.J.N., HAINES, M.G., PORTONE, A., Nucl. Fusion **37** (1997) 1679.

[12] ALBANESE, R. and VILLONE, F., Nucl. Fusion **38** (1998) 723.

[13] VILLONE, F., VYAS, P., LISTER, J.B., ALBANESE, R., Nucl. Fusion **37** (1997) 1395.

[14] VYAS, P., VILLONE, F., LISTER, J.B., ALBANESE, R., Rep. LRP 583/97, CRPP, Lausanne (1997), accepted for publication in Nucl. Fusion

[15] LJUNG, L., *System Identification: Theory for the user*, Prentice-Hall (1987)

[16] YOSHIOKA, K., ABE, M., KOBAYASHI, T., Jpn. J. Appl. Phys. **21** 10 (1982) 1501.

[17] EMAAMI, M., WOOD, H.C., HIROSE, A., SKASGARD, H.M., IEEE Trans. Industrial Electronics **37** (1990) 317

[18] LISTER, J.B., LAZARUS, E.A., KELLMAN, A.G., MORET, J-M. FERRON, J.R. et al., Nucl. Fusion **30** (1990) 2349.

[19] VYAS, P., 'Plasma Vertical Position Control in the COMPASS-D Tokamak', D.Phil. Thesis, University of Oxford, 1996.

[20] LISTER, J.B., et al., Proc. 36th IEEE Conf. Decision and Control, San Diego, USA, December 1997 (1997) 3679; Rep. LRP 584/97, CRPP, Lausanne (1997).

[21] COUTLIS, A., et al., Proc. 36th IEEE Conf. Decision and Control, San Diego, USA, December 1997 (1997) 3685; Rep. LRP 584/97, CRPP, Lausanne (1997).

[22] COUTLIS, A., PhD Thesis, Univ. of London, Imperial College of Science, Technology and Medicine, 1997.

[23] COUTLIS, A., LIMEBEER, D.J.N., WAINWRIGHT, J. P., LISTER, J.B., VYAS, P., Submitted to IEEE Trans. Applications Control Systems

Appendix A COUTLIS, A., et al., Rep. LRP 606/98, CRPP, Lausanne (1998).

[24] LISTER, J.B., et al., Fusion Technol. **32** (1997) 321

[25] ALBANESE, R., BLUM, J., DE BARBIERI, O., 'Numerical Studies of the Next European Torus via the PROTEUS Code,' presented at the. 12th Conf. Numerical Simulation of Plasmas, San Francisco, California, Sept. 20-23, 1987

[26] HOFMANN, F., TONETTI, G., Nucl. Fusion **28** (1988) 1871.

FIGURES

Figure 1 The TCV vacuum vessel, poloidal field coils, poloidal field probes (denoted by dashes inside the tiles) and flux loops (denoted by crosses). The last closed flux surface of the nominal plasma is shown (discharge 13333).

Figure 2 Schematic Diagram of the TCV feedback control loop.

Figure 4 Plasma response to multi-sinusoidal stimulation (discharge 13333), showing the sinusoidal stimulation signal, the measured (solid curve) and fitted coil (dashed curve) responses of power supply demand voltages and zI_p signal, and the measurement-fit residuals.

Figure 5 Measured frequency components of coil voltage signal (crosses) and zI_p response (circles).

Figure 3 Comparison of modelled (curves) and measured (crosses and circles) frequency responses of the plasma-less system. Solid curves and crosses represent flux loop #22 (outboard side, closest to PF coil F4). Dashed curves and circles represent flux loop #38 (inboard side, closest to PF coil E4).

Figure 6 The frequency response of zI_p to antisymmetric stimulation of PF coils E4-E5 (circles) and F1-F8 (crosses). The solid lines represent the CREATE-L model, dashed lines represent the RZIP model, and the dotted lines represent the low order system identified model.

Figure 7 Frequency responses representing a) good agreement between the measured and RZIP and CREATE-L predictions, b) good agreement between the measured and plasma-less predictions, and c) BGBM improvement. The measured frequency responses are marked as circles, the plasma-less model is the dashed line, The RZIP model is the line marked by crosses (×), the CREATE-L model is the solid line, and the BGBM model is the line marked by pluses (+).

Figure 8 The variation of the vertical field and net poloidal flux provided by current changes in the different TCV PF coils.

Figure 9 The response to decoupled stimulation.

Figure 10 Cost function variation with plasma related elements of the circuit equations.

Figure 11 Cost function variation with the power supply time constant and the number of eigenmodes in the RZIP model.

Figure 12 The extreme plasma shapes for which the RZIP model was calculated.

Figure 13 The variation of the RZIP model for the equilibria in Fig. 12. The cases illustrated are a) the stimulation of P_VERT and I_p demonstrating insensitivity to plasma triangularity, and b) the stimulation of Ψ_R and TRI_IN showing weak sensitivity to plasma elongation.

Figure 14 Simplified current profiles used for calculation of the RZIP-0 models.

Figure 15 Transfer functions for the nominal RZIP model (circles), the model with circular current distribution (solid curves) and the model with elliptical profile (dashed curves).

TABLES

Table TABEXTREQUIL. Variation of the RZIP Parameters for the Shapes Illustrated in Figure 12.

Discharge	κ_{95}	δ_{95}	I_p[kA]	M_{33}	M_{34}	M_{43}	L_{p0}
11961	1.5	-0.22	250	-3.88×10^{-6}	1.70×10^{-6}	1.76×10^{-6}	1.91×10^{-6}
12012	1.55	0.35	402	-3.48×10^{-6}	1.49×10^{-6}	1.78×10^{-6}	1.72×10^{-6}
9849	1.18	0.02	230	-2.24×10^{-6}	1.65×10^{-6}	2.16×10^{-6}	2.24×10^{-6}
10007	1.83	0.01	522	-3.57×10^{-6}	1.42×10^{-6}	1.78×10^{-6}	1.71×10^{-6}

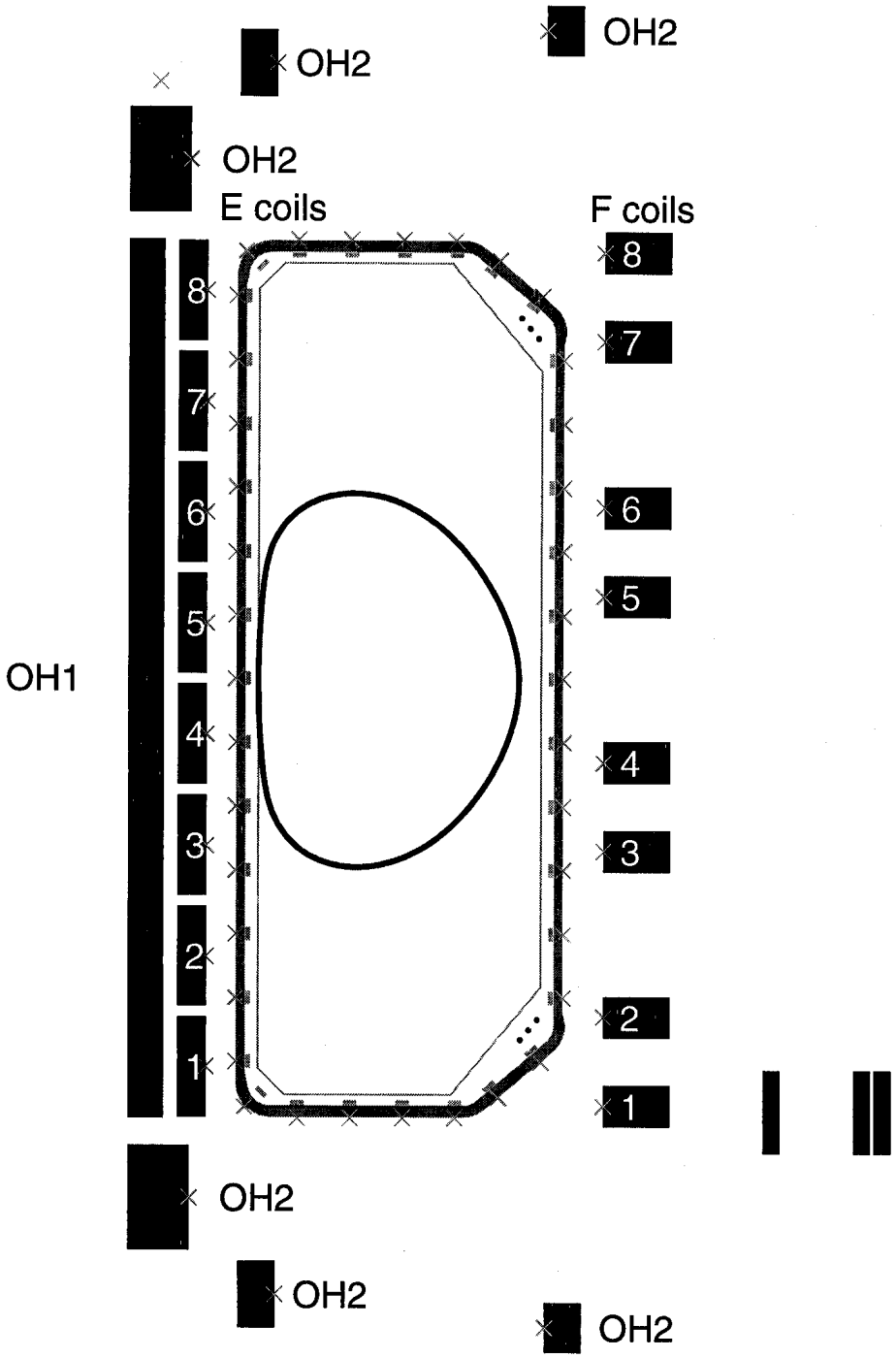

FIG. 1. The TCV vacuum vessel, poloidal field coils, poloidal field probes (denoted by dashes inside the tiles) and flux loops (denoted by crosses). The last closed flux surface of the nominal plasma is shown (discharge 13333).

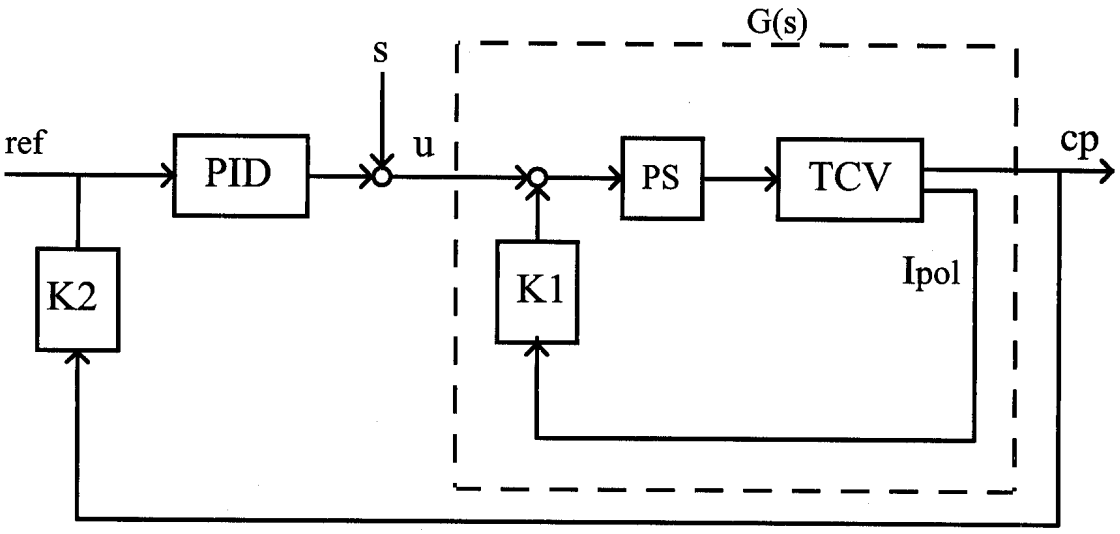

FIG. 2. Schematic Diagram of the TCV feedback control loop.

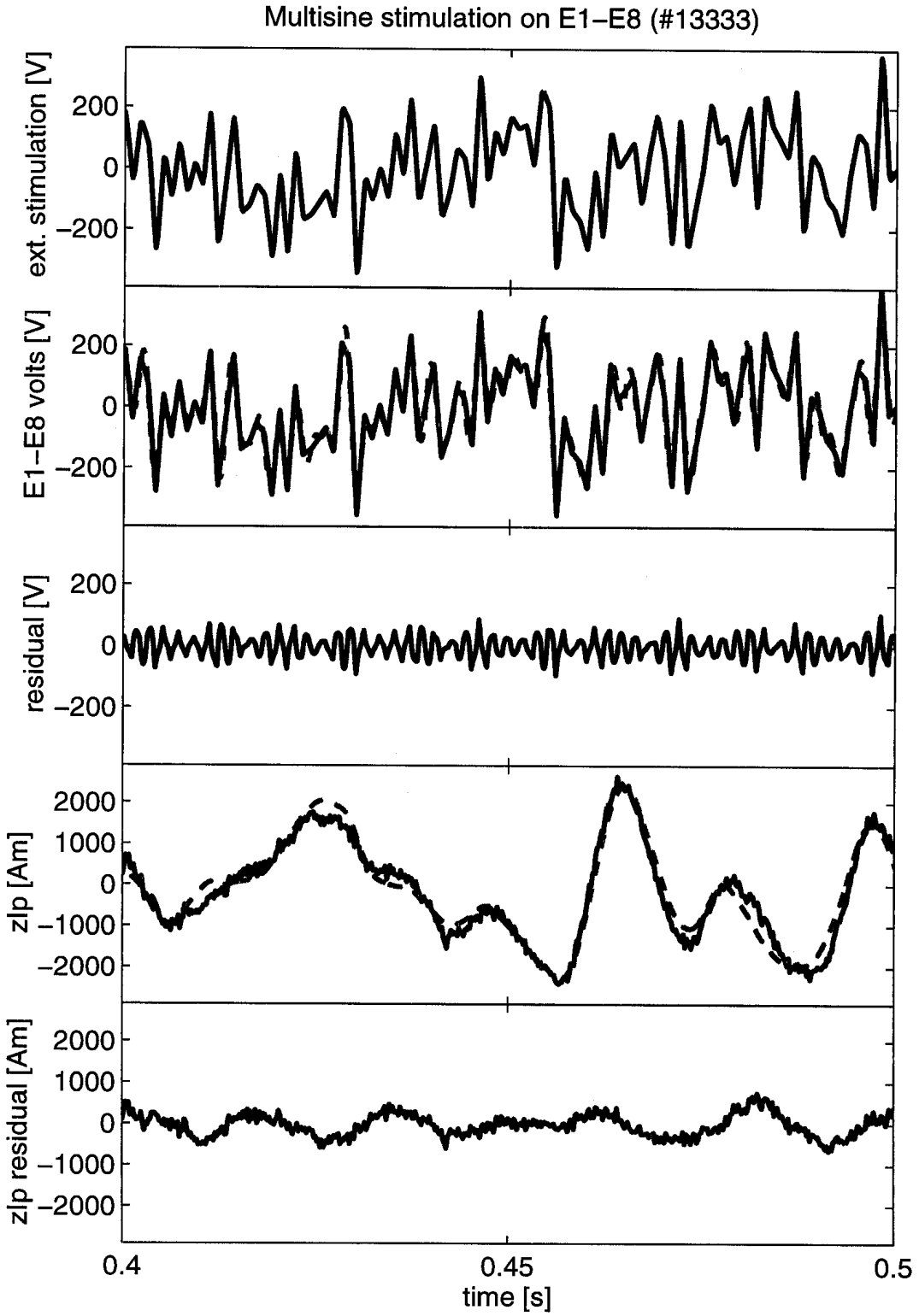

FIG. 4. Plasma response to multi-sinusoidal stimulation (discharge 13333), showing the sinusoidal stimulation signal, the measured (solid curve) and fitted coil (dashed curve) responses of power supply demand voltages and zI_p signal, and the measurement-fit residuals.

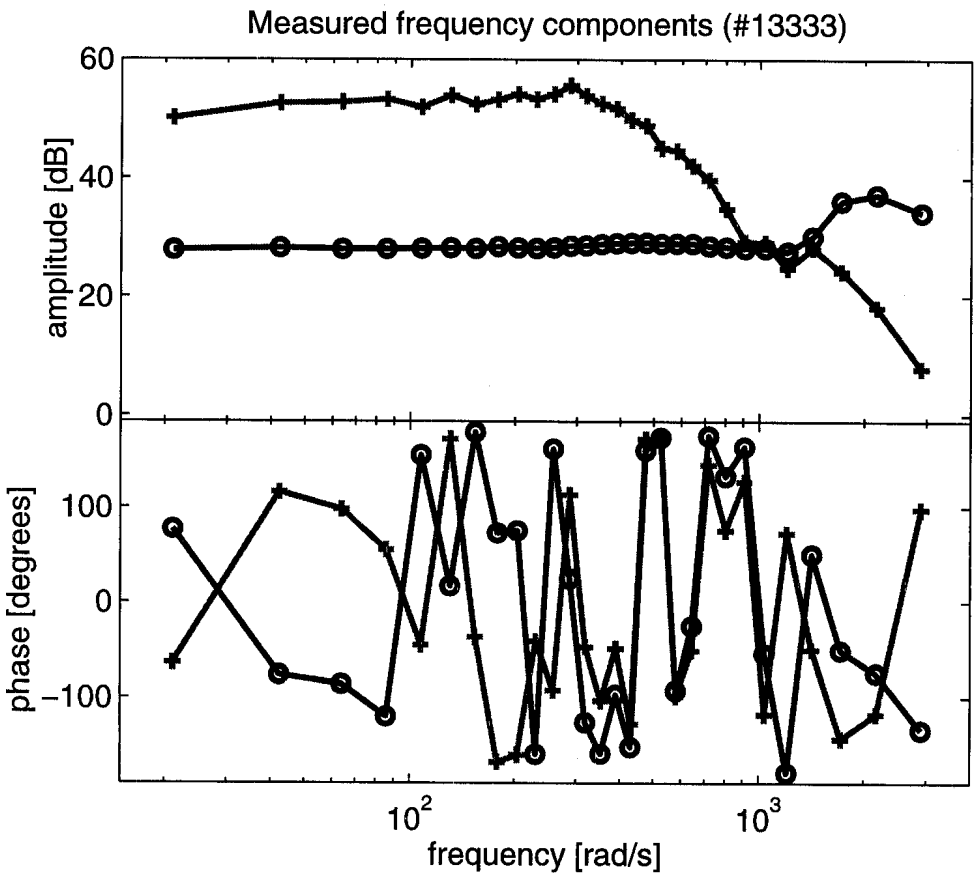

FIG. 5. Measured frequency components of coil voltage signal (crosses) and zI_p response (circles).

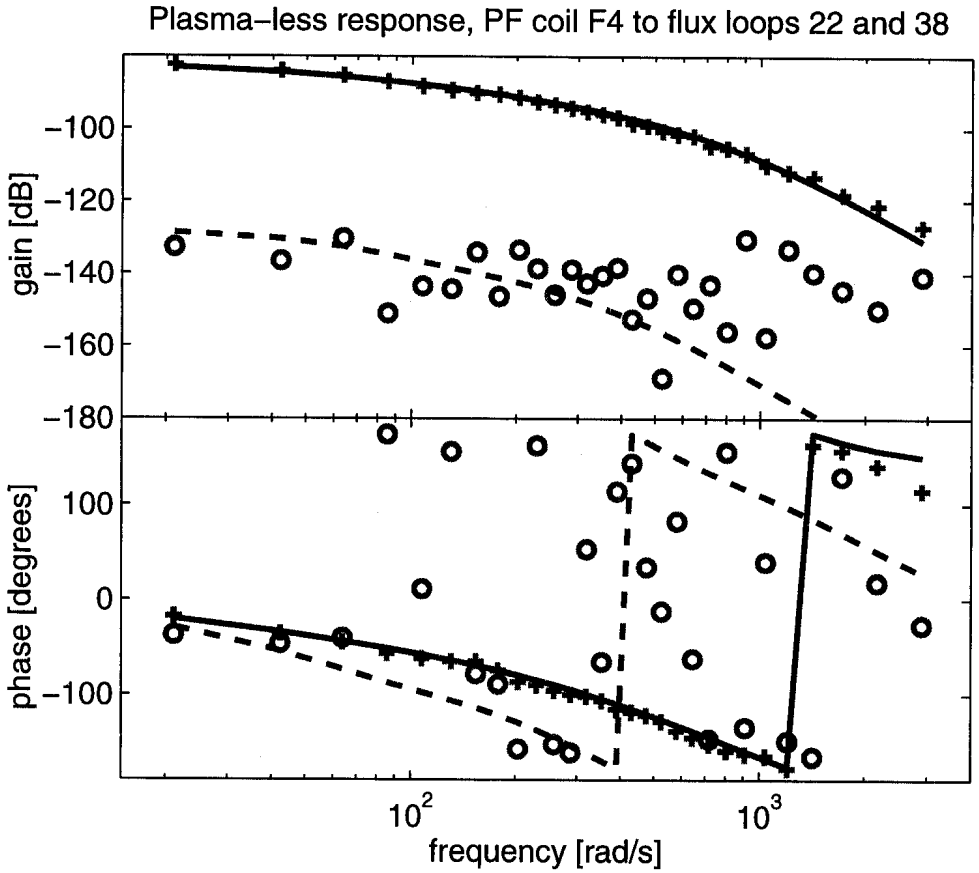

FIG. 3. Comparison of modelled (curves) and measured (crosses and circles) frequency responses of the plasma-less system. Solid curves and crosses represent flux loop #22 (outboard side, closest to PF coil F4). Dashed curves and circles represent flux loop #38 (inboard side, closest to PF coil E4).

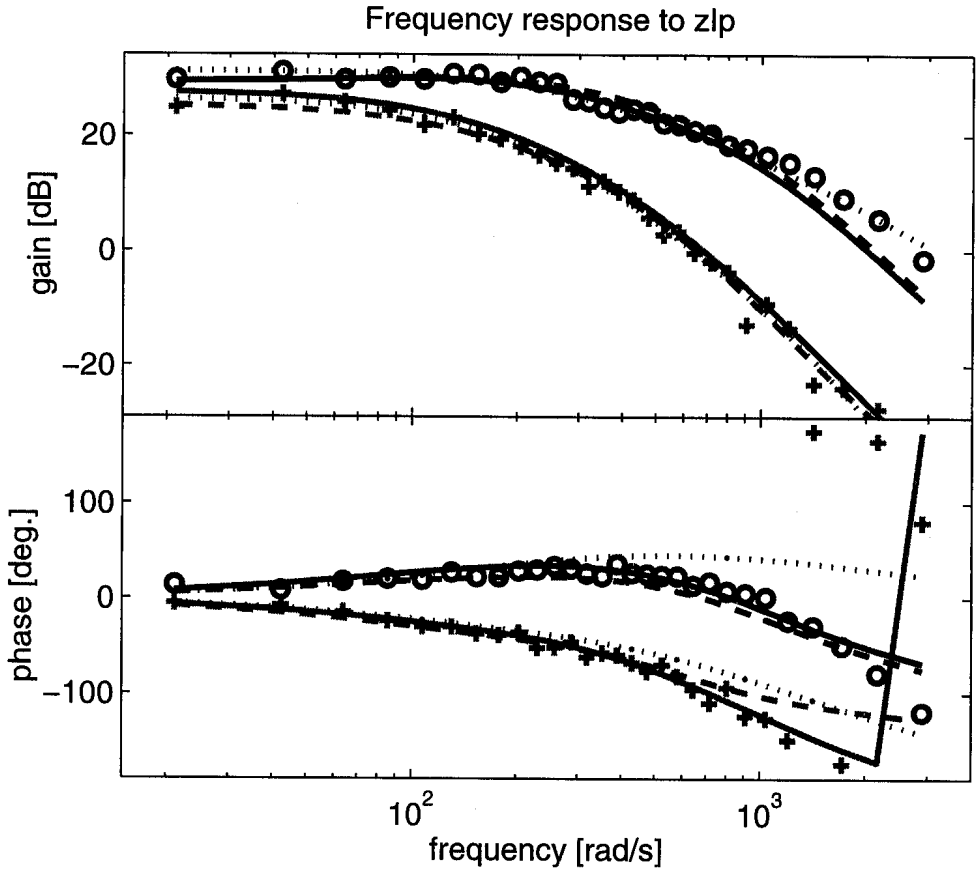

FIG. 6. The frequency response of zI_p to antisymmetric stimulation of PF coils E4-E5 (circles) and F1-F8 (crosses). The solid lines represent the CREATE-L model, dashed lines represent the RZIP model, and the dotted lines represent the low order system identified model.

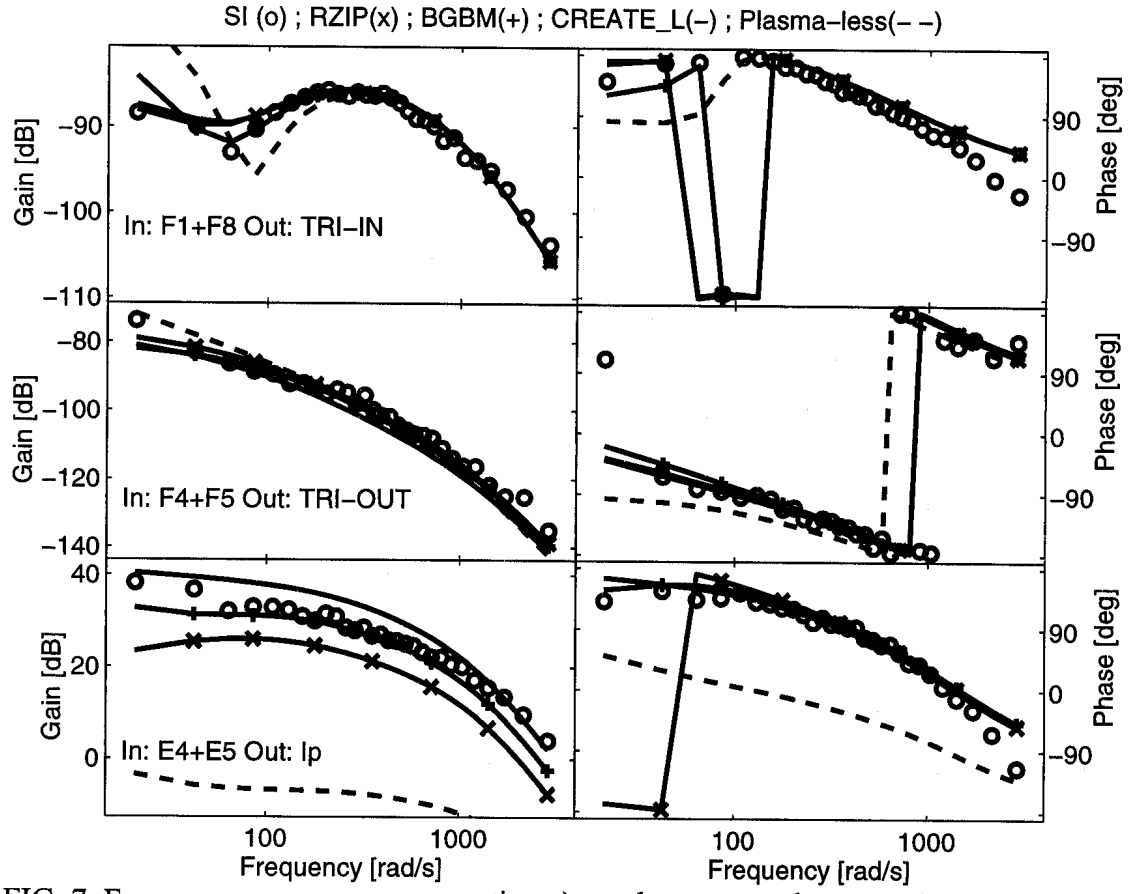

FIG. 7. Frequency responses representing a) good agreement between the measured and RZIP and CREATE-L predictions, b) good agreement between the measured and plasma-less predictions, and c) BGBM improvement. The measured frequency responses are marked as circles, the plasma-less model is the dashed line, The RZIP model is the line marked by crosses (×), the CREATE-L model is the solid line, and the BGBM model is the line marked by pluses (+).

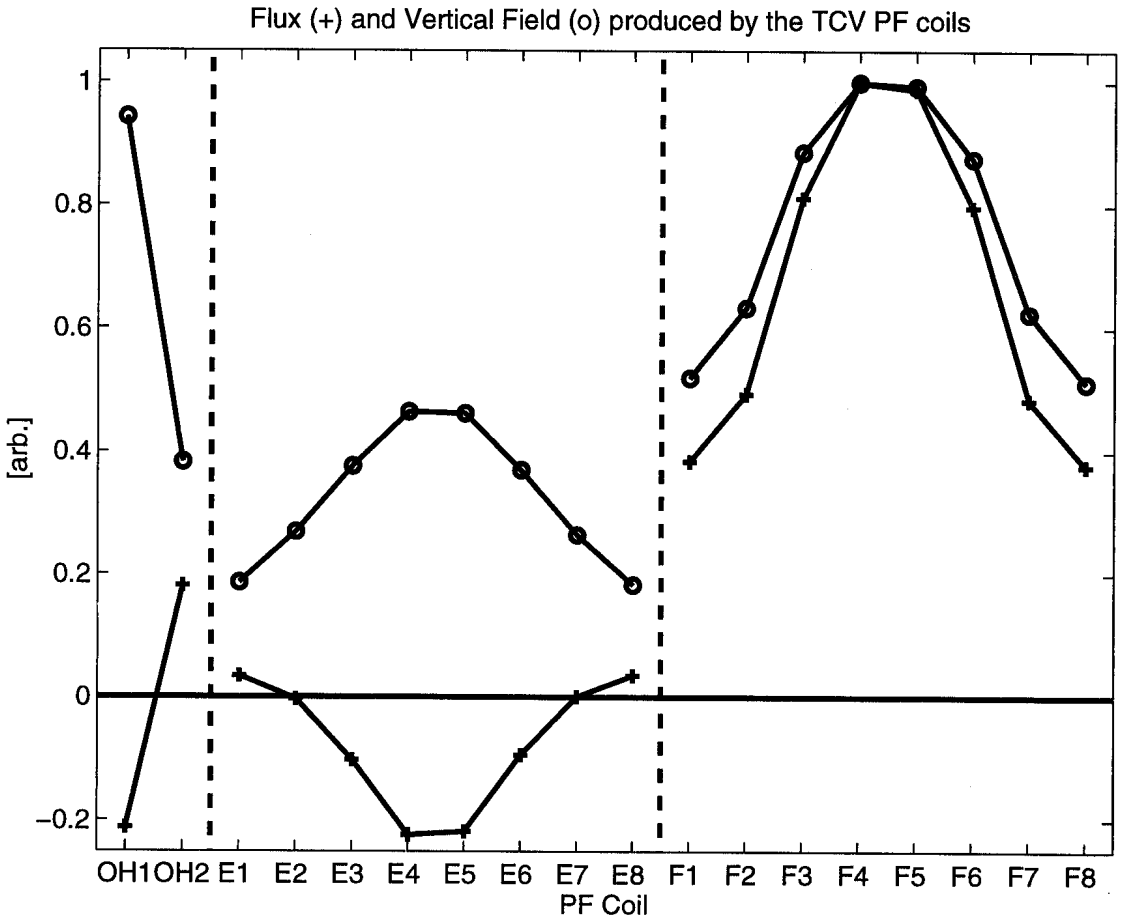

FIG. 8. The variation of the vertical field and net poloidal flux provided by current changes in the different TCV PF coils.

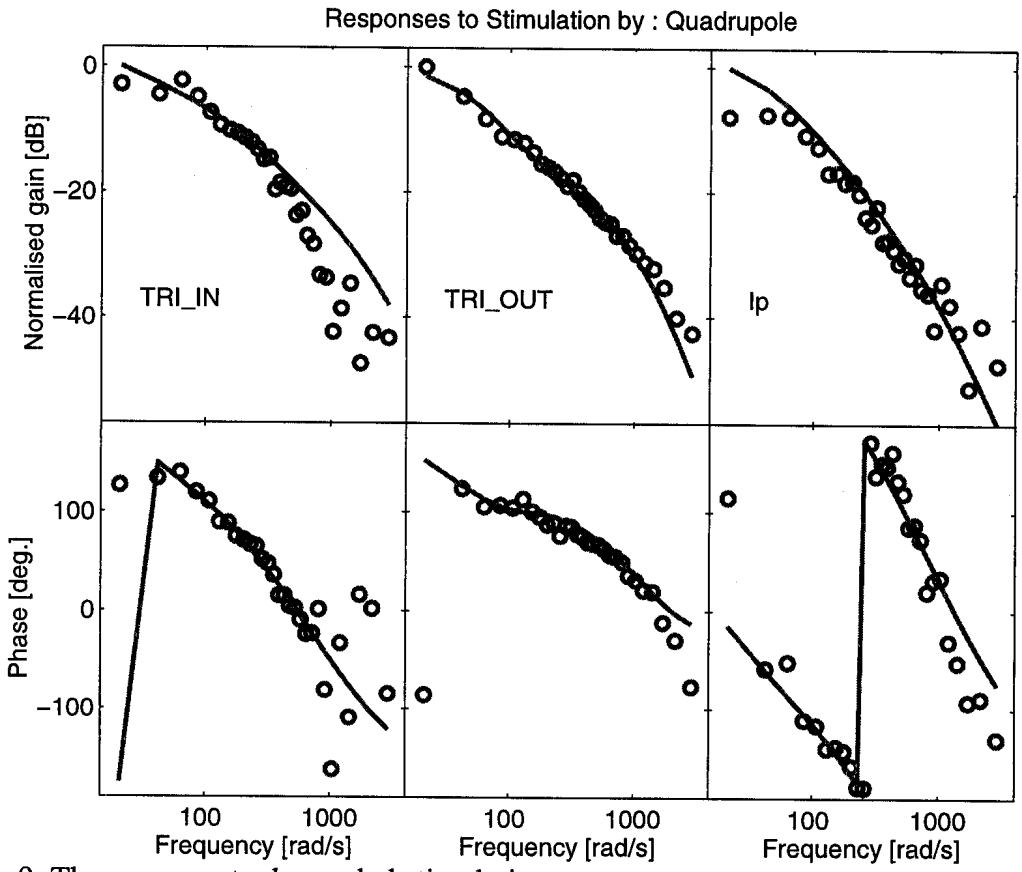

FIG. 9. The response to decoupled stimulation.

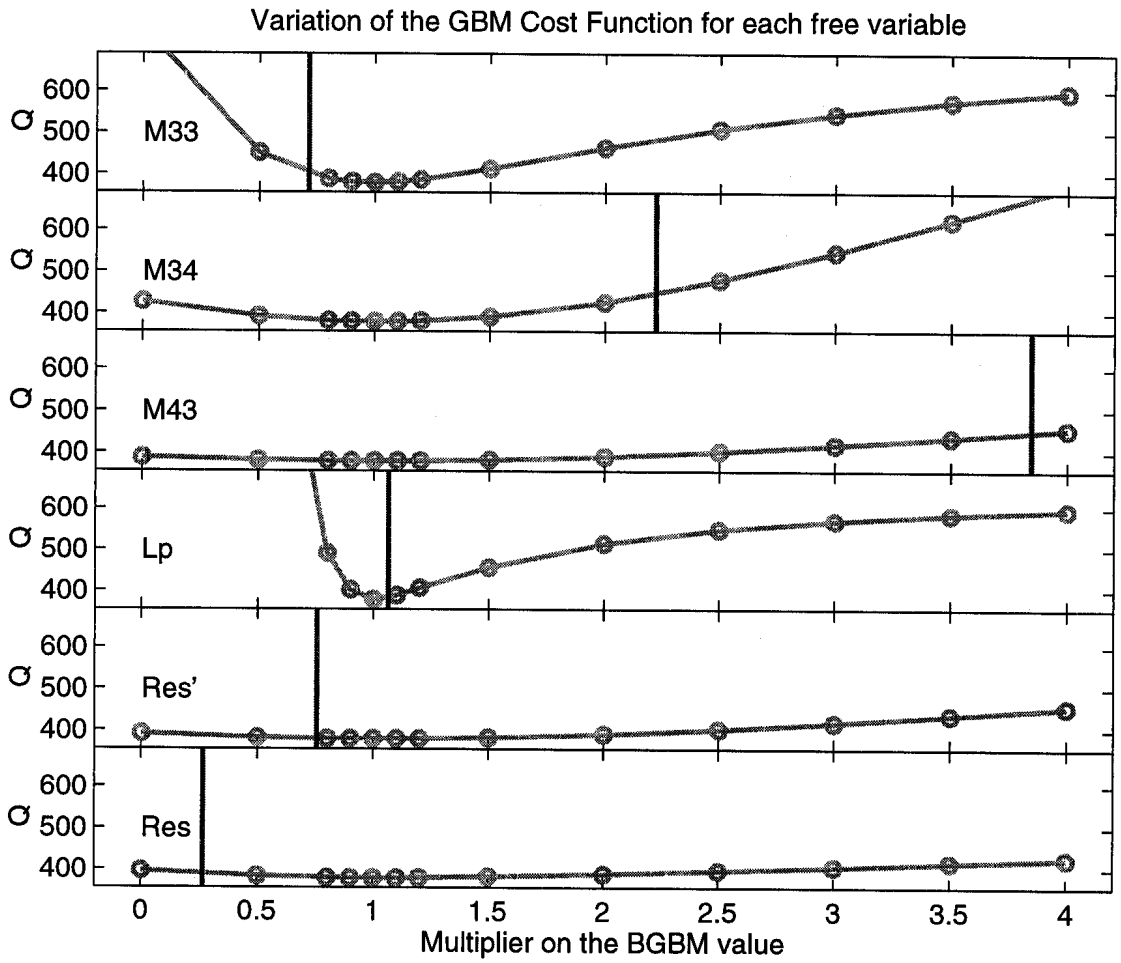

FIG. 10. Cost function variation with plasma related elements of the circuit equations.

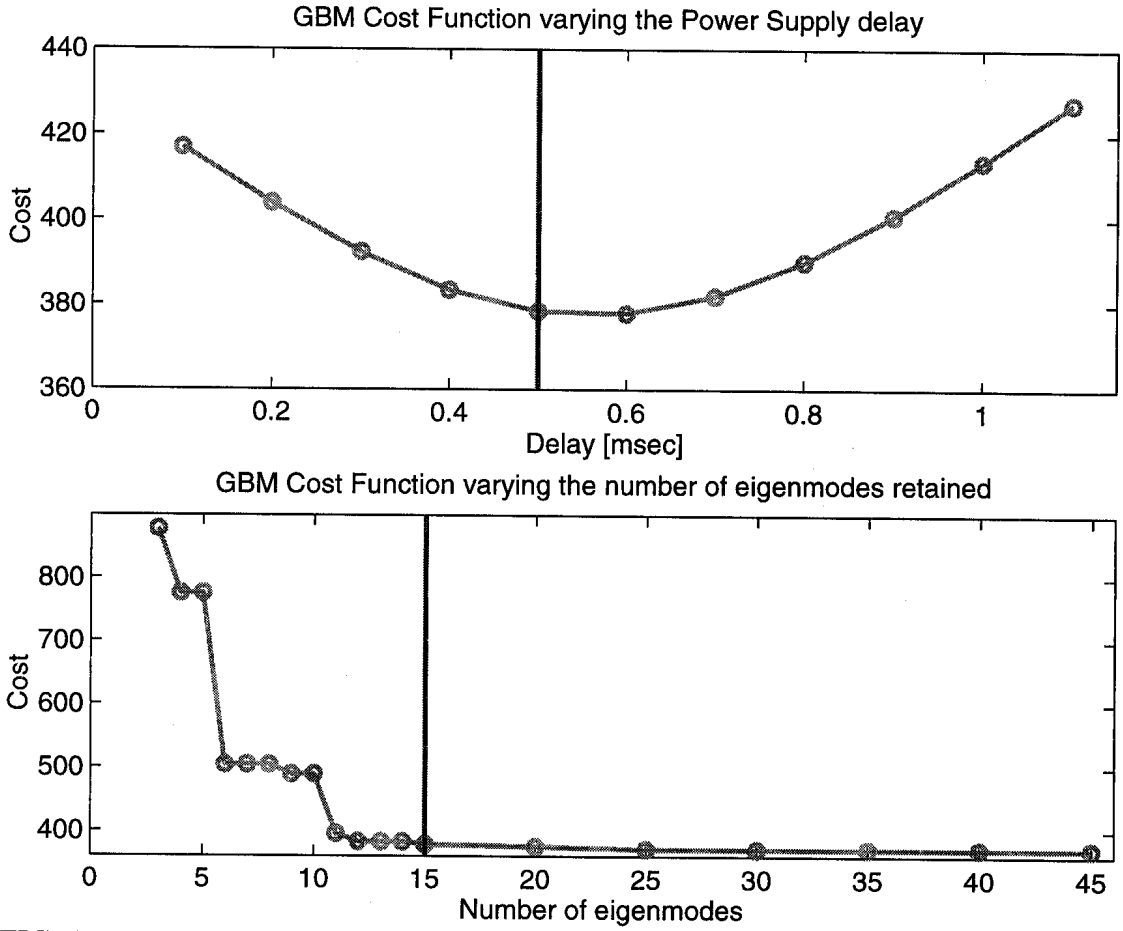

FIG. 11. Cost function variation with the power supply time constant and the number of eigenmodes in the RZIP model.

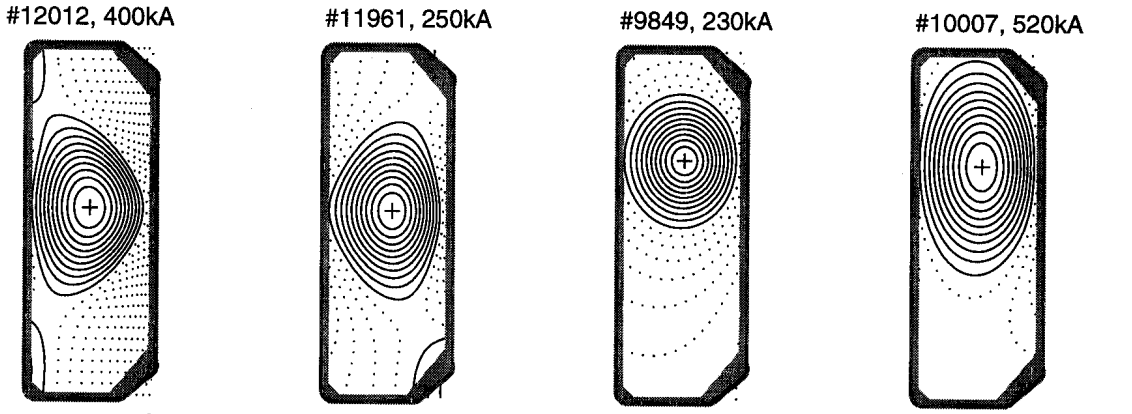

FIG. 12. The extreme plasma shapes for which the RZIP model was calculated.

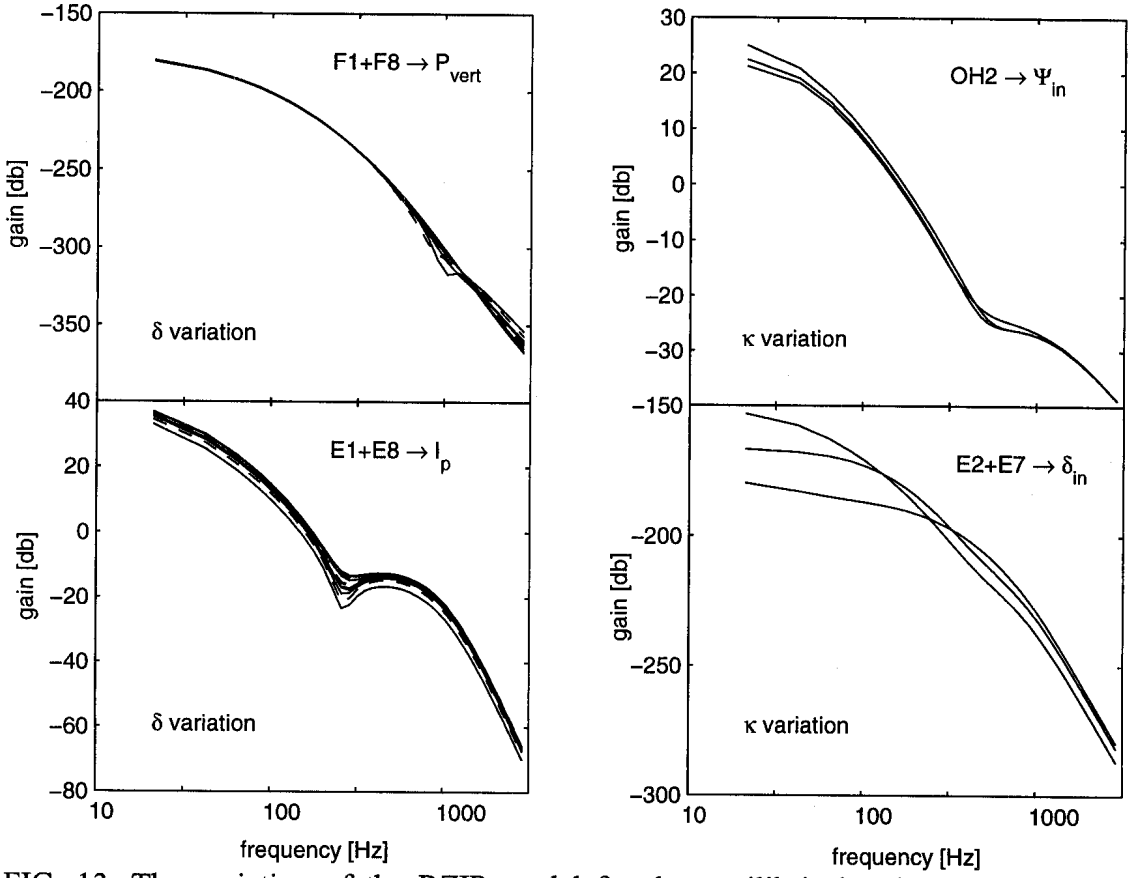

FIG. 13. The variation of the RZIP model for the equilibria in Fig. 12. The cases illustrated are a) the stimulation of P_VERT and I_p demonstrating insensitivity to plasma triangularity, and b) the stimulation of Ψ_R and TRI_IN showing weak sensitivity to plasma elongation.

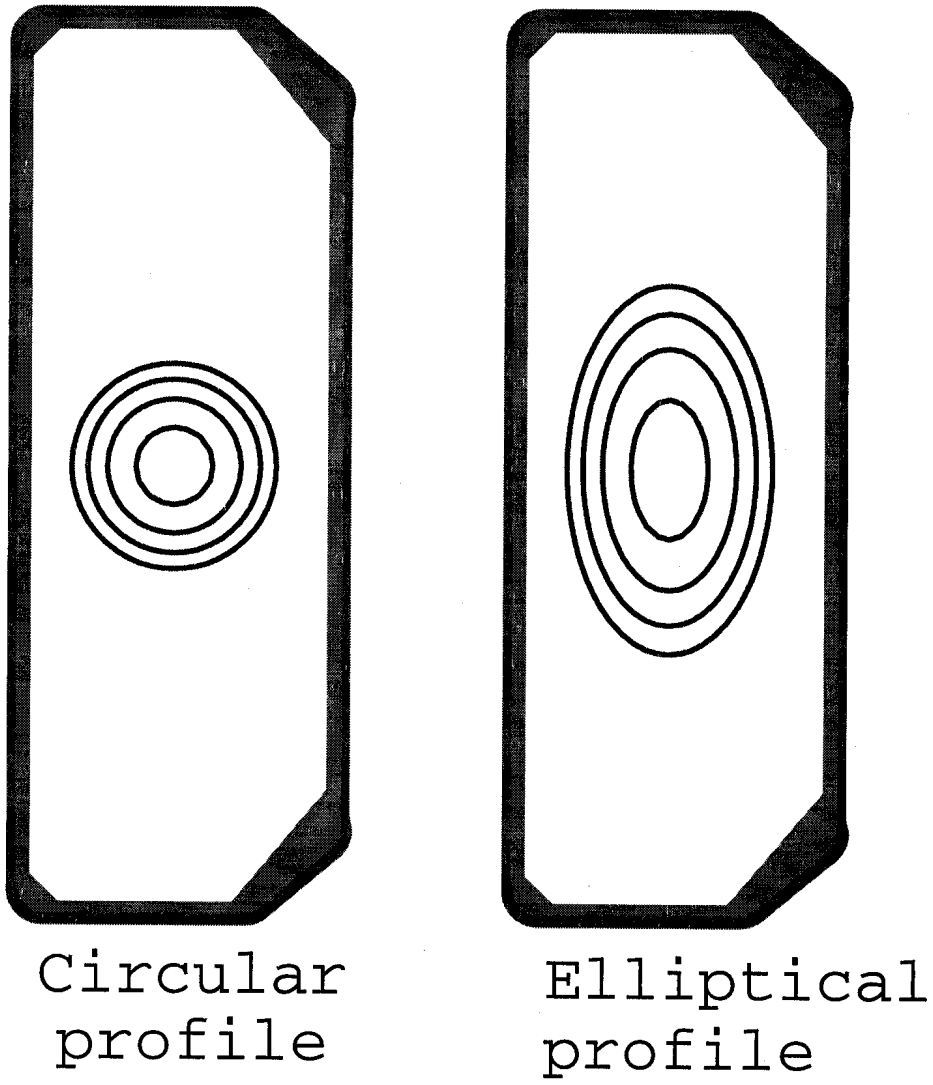

FIG. 14. Simplified current profiles used for calculation of the RZIP-0 models.

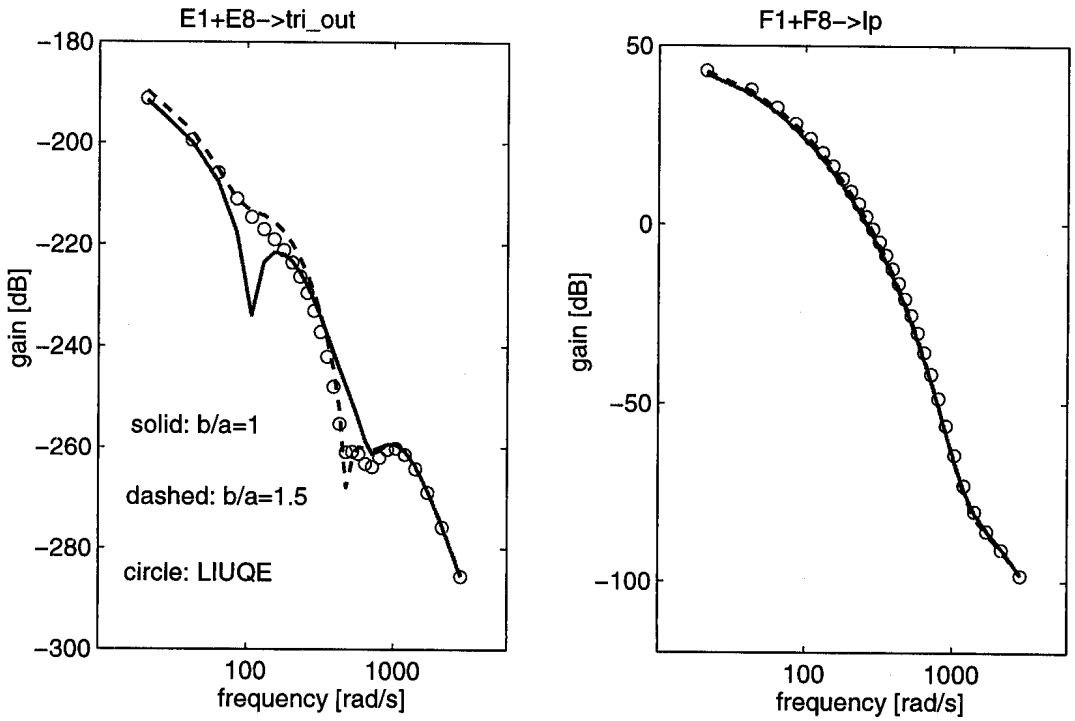

FIG. 15. Transfer functions for the nominal RZIP model (circles), the model with circular current distribution (solid curves) and the model with elliptical profile (dashed curves).

APPENDIX A

This Appendix records a more complete comparison between the system identified frequency response estimates and the CREATE-L and RZIP models. Figures A1 and A2 show the zI_p frequency responses to antisymmetric stimulation. For E coil stimulation, the amplitude responses of the two models are indistinguishable and have excellent agreement with the data. Differences of the order of 10° can be seen in the phase responses, but this is always within the variance of the experimental estimates. The low frequency gain of the two models differ for the F coil responses, but again this is within the variance of the data.

Figures A3 to A12 present the responses to symmetric stimulation. The main features are summarised in Sections 4.4 and 5.3.

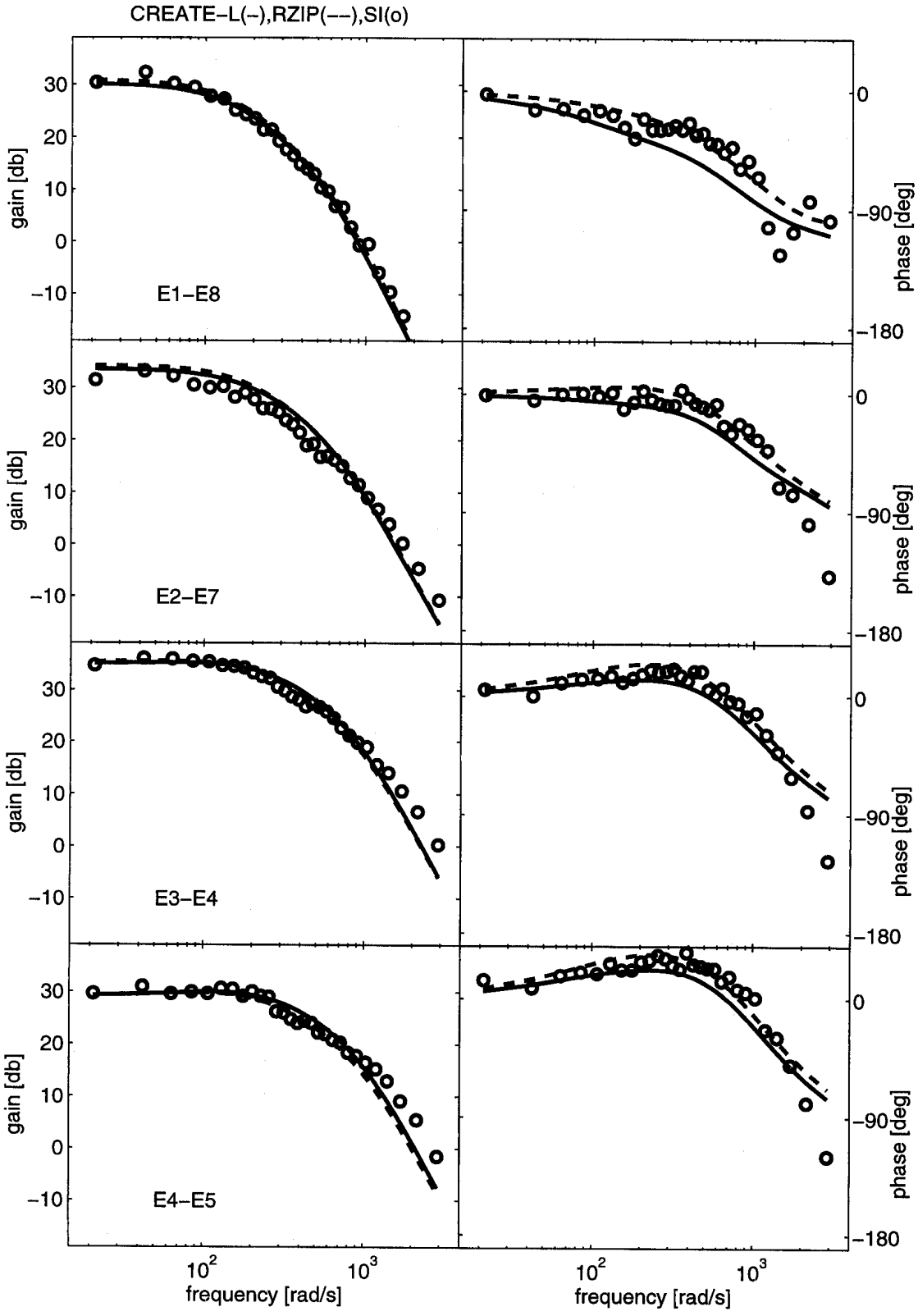

FIG. A1. Frequency response of zI_p to antisymmetric stimulation on the E coils. The system identified estimates are indicated by circles, the CREATE-L response is indicated by a solid line and RZIP by a dashed line.

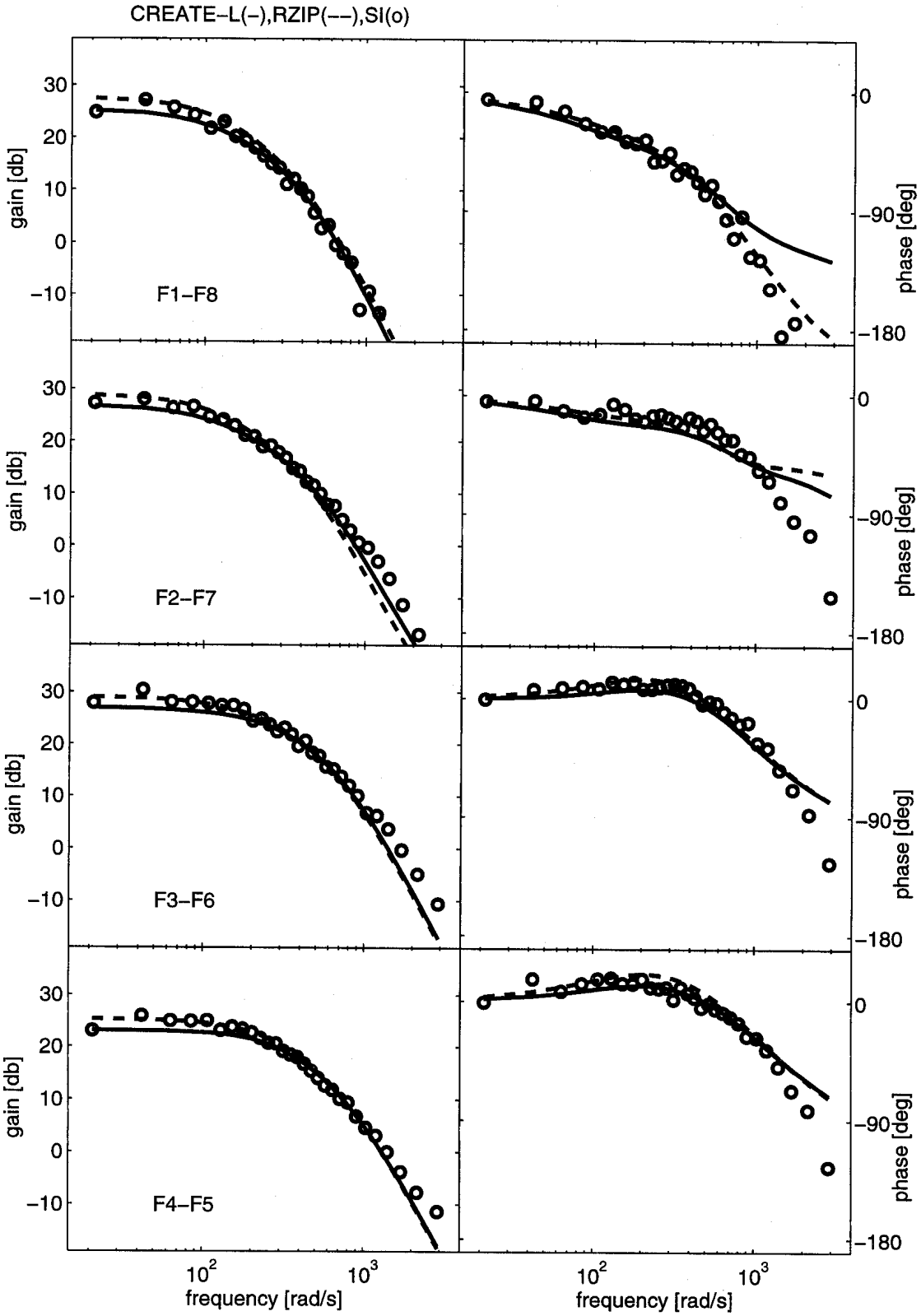

FIG. A2. Frequency response of zI_p to antisymmetric stimulation on the F coils. The system identified estimates are indicated by circles, the CREATE-L response is indicated by a solid line and RZIP by a dashed line.

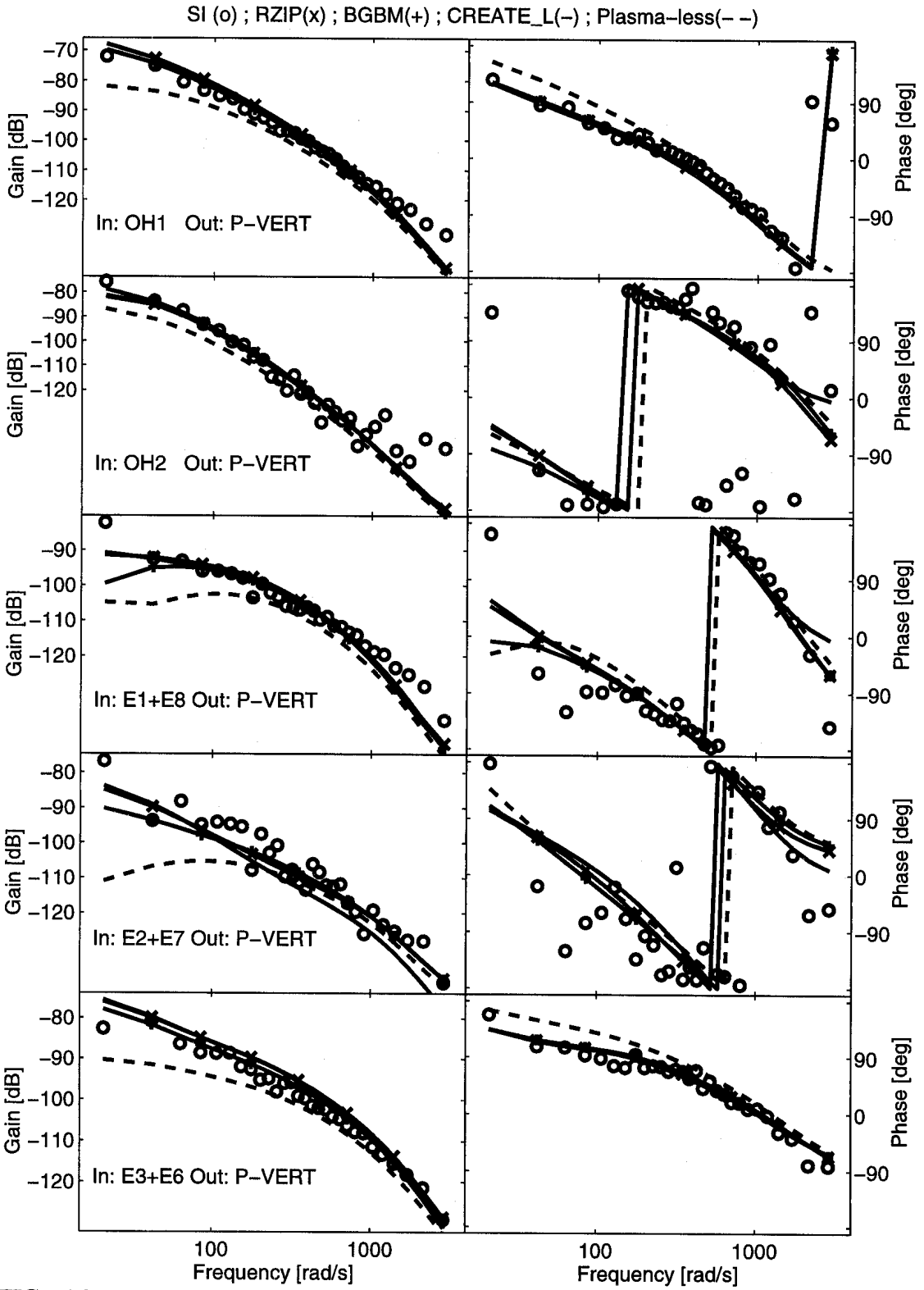

FIG. A3. Frequency response of P_VERT to symmetric stimulation. The system identified estimates are indicated by circles, the CREATE-L response is indicated by a solid line, RZIP by a line with diagonal crosses, the BGBM response by a line with vertical crosses, and the plasma-less model by a dashed line.

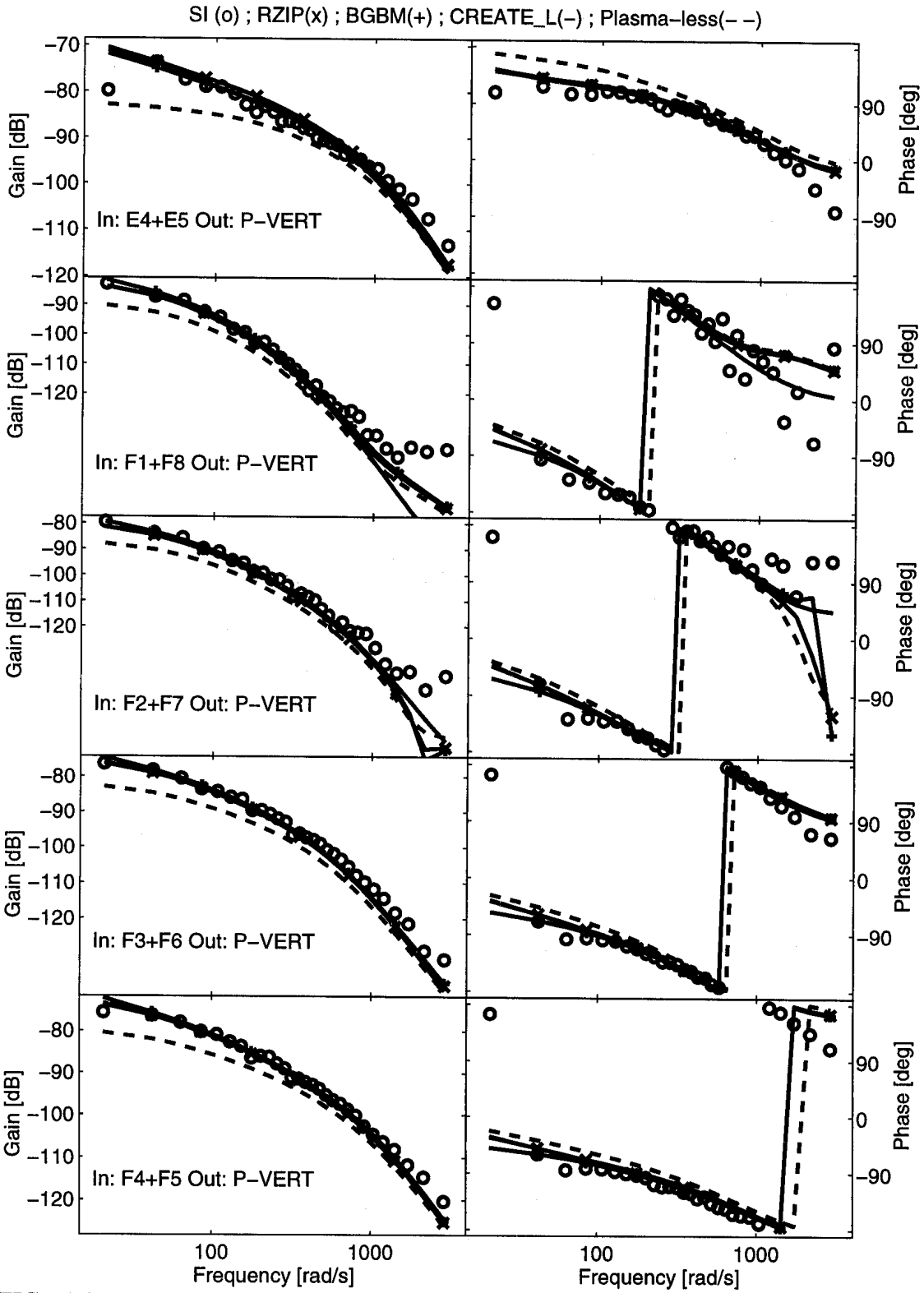

FIG. A4. Frequency response of P_VERT to symmetric stimulation. The system identified estimates are indicated by circles, the CREATE-L response is indicated by a solid line, RZIP by a line with diagonal crosses, the BGBM response by a line with vertical crosses, and the plasma-less model by a dashed line.

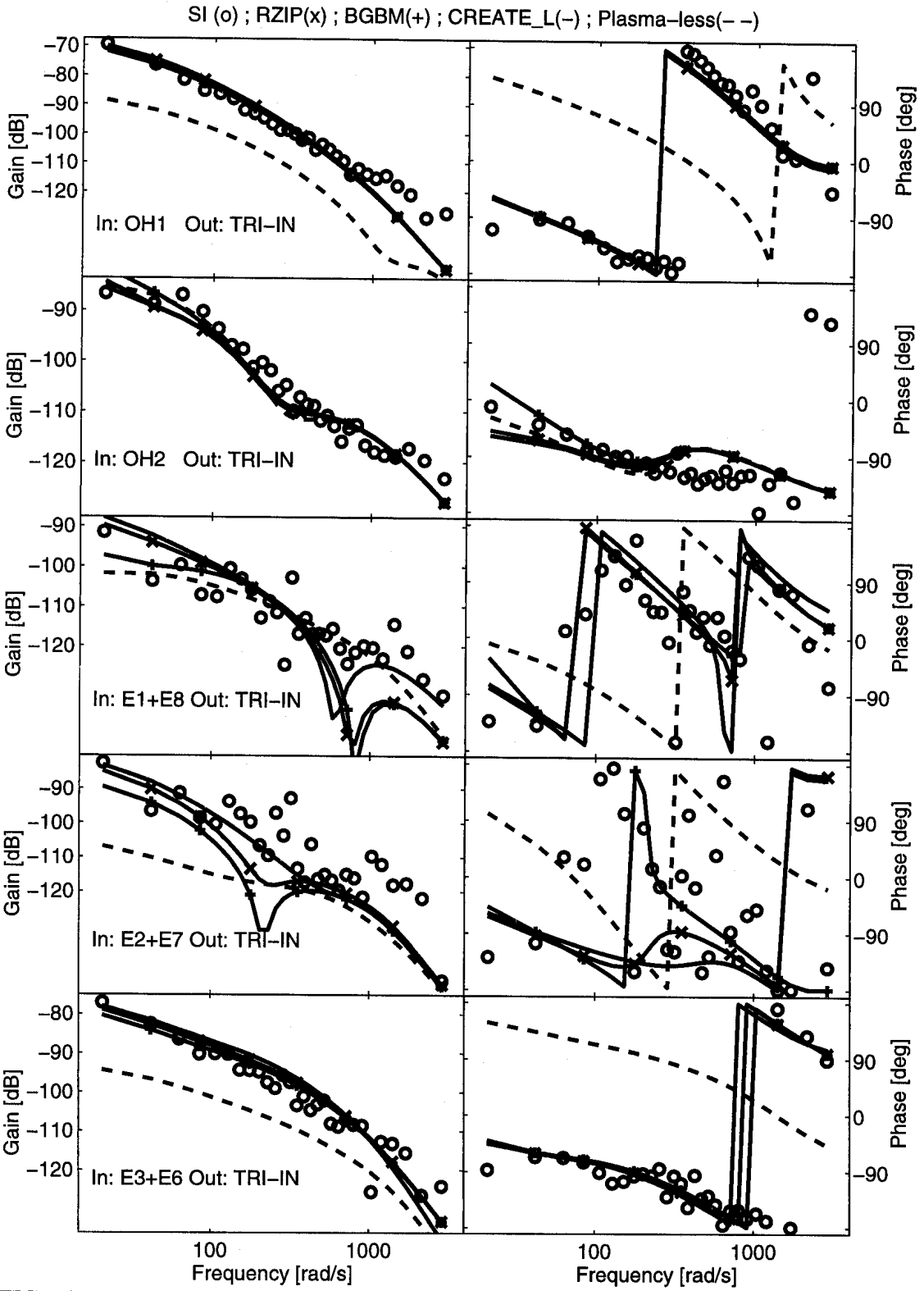

FIG. A5. Frequency response of TRI_IN to symmetric stimulation. The system identified estimates are indicated by circles, the CREATE-L response is indicated by a solid line, RZIP by a line with diagonal crosses, the BGBM response by a line with vertical crosses, and the plasma-less model by a dashed line.

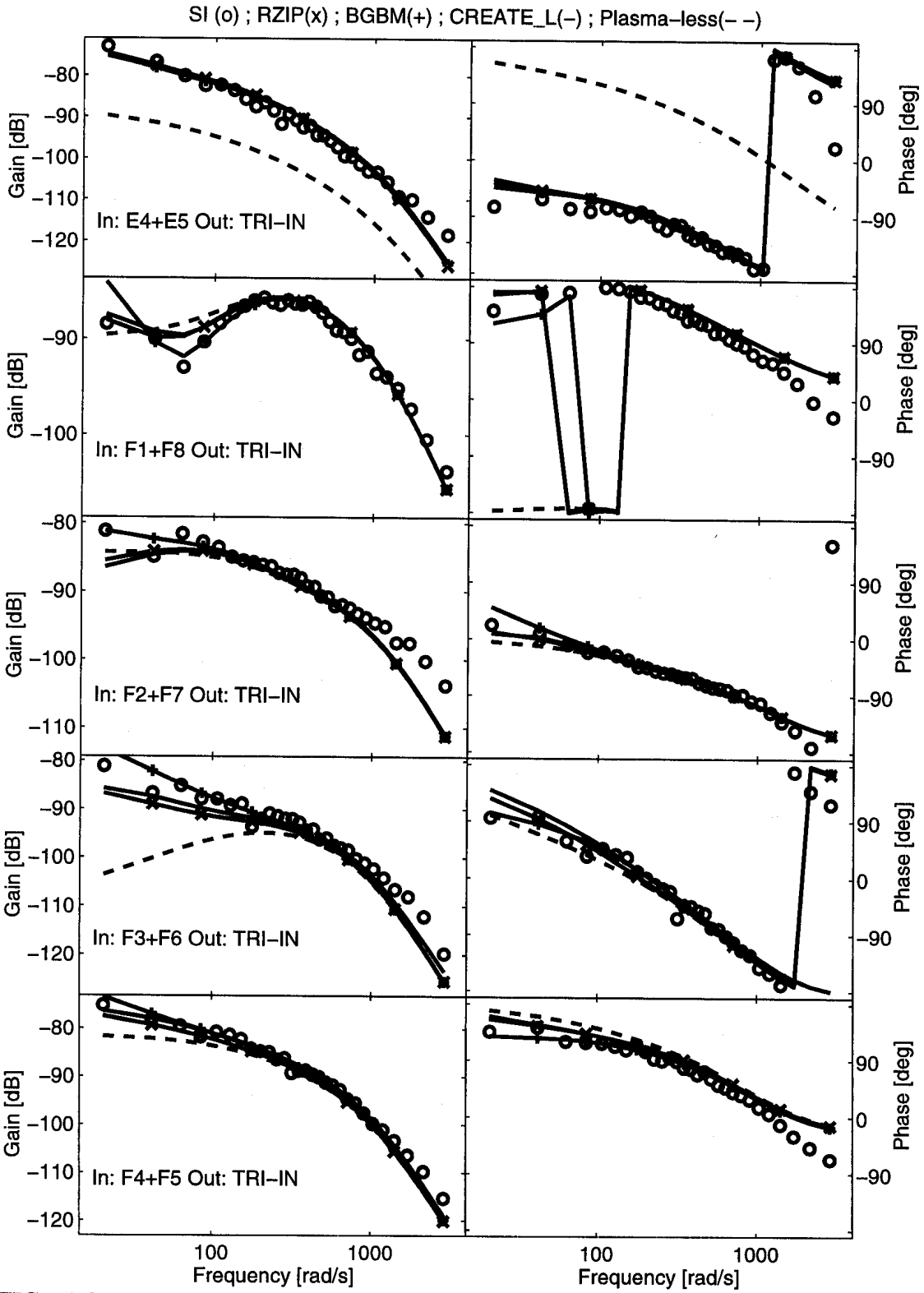

FIG. A6. Frequency response of TRI_IN to symmetric stimulation. The system identified estimates are indicated by circles, the CREATE-L response is indicated by a solid line, RZIP by a line with diagonal crosses, the BGBM response by a line with vertical crosses, and the plasma-less model by a dashed line.

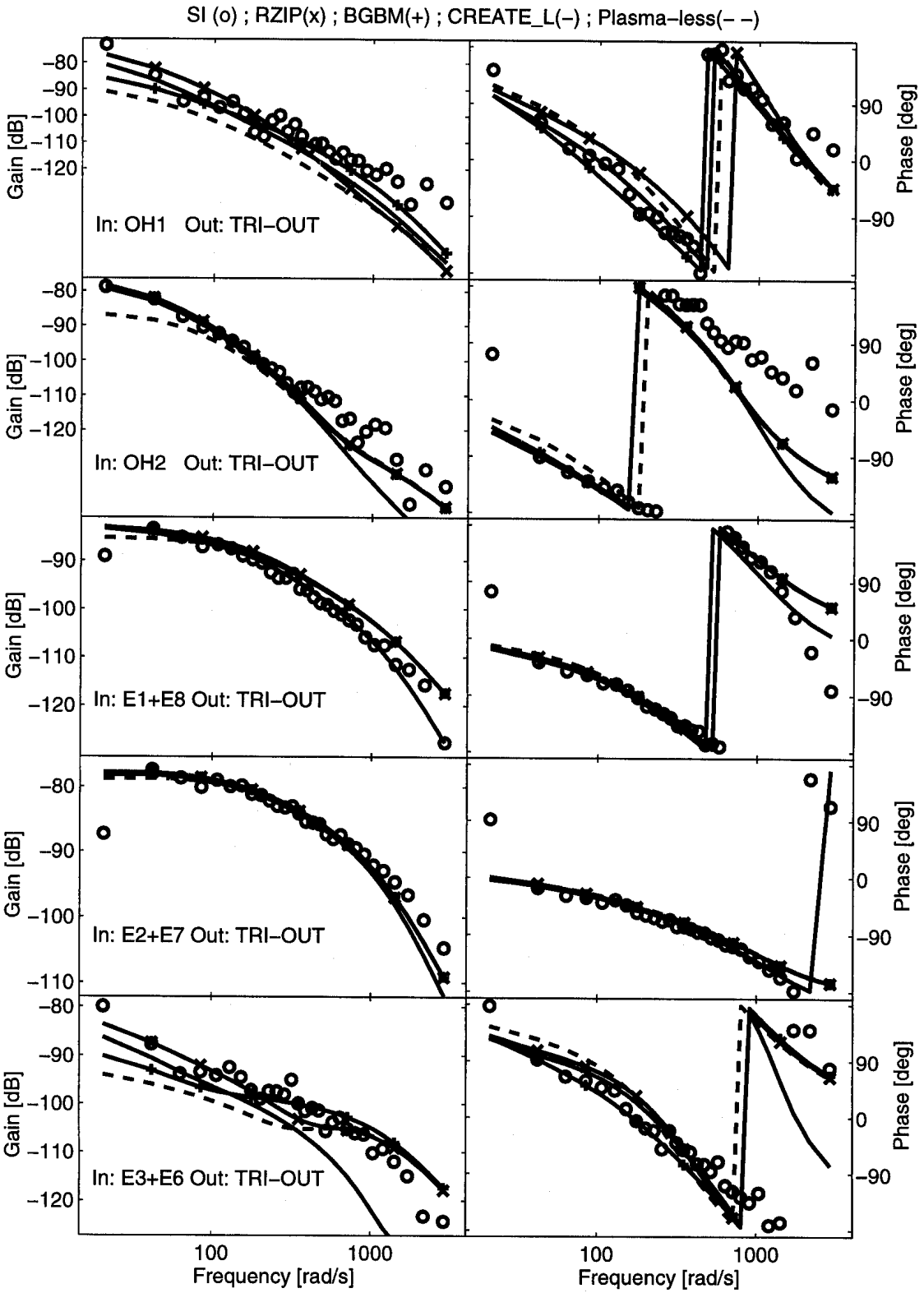

FIG. A7. Frequency response of TRI_OUT to symmetric stimulation. The system identified estimates are indicated by circles, the CREATE-L response is indicated by a solid line, RZIP by a line with diagonal crosses, the BGBM response by a line with vertical crosses, and the plasma-less model by a dashed line.

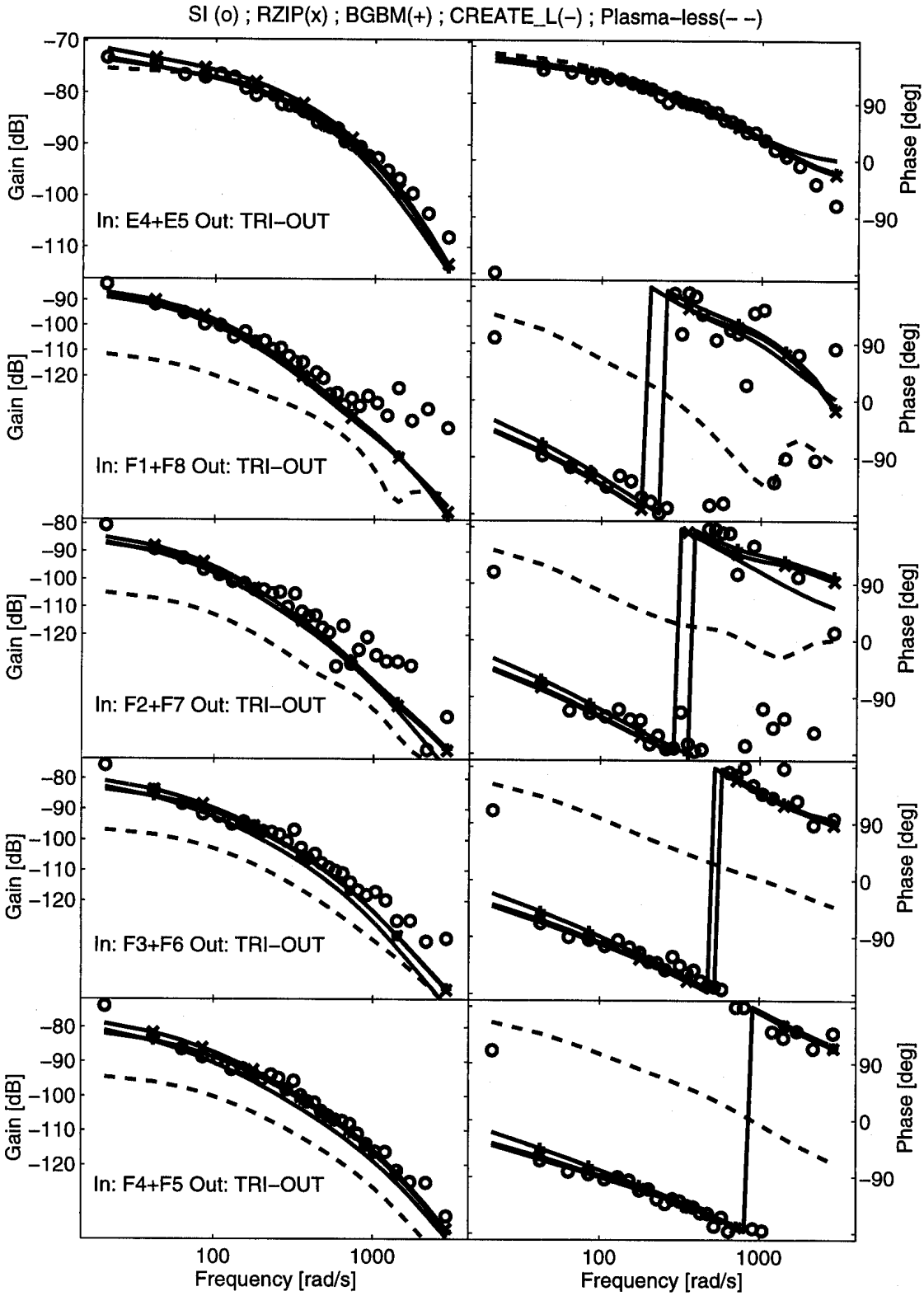

FIG. A8. Frequency response of TRI_OUT to symmetric stimulation. The system identified estimates are indicated by circles, the CREATE-L response is indicated by a solid line, RZIP by a line with diagonal crosses, the BGBM response by a line with vertical crosses, and the plasma-less model by a dashed line.

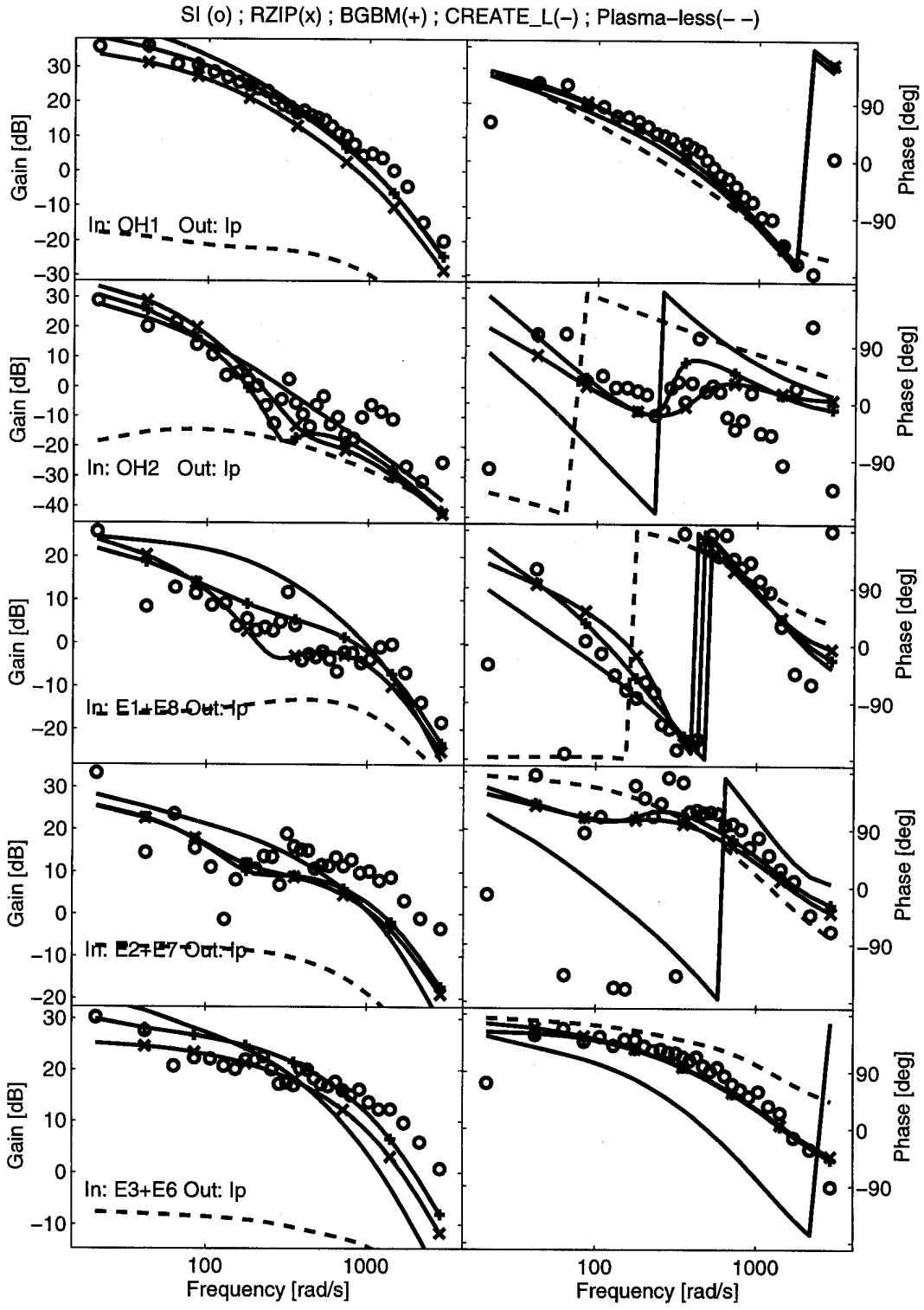

FIG. A9. Frequency response of I_p to symmetric stimulation. The system identified estimates are indicated by circles, the CREATE-L response is indicated by a solid line, RZIP by a line with diagonal crosses, the BGBM response by a line with vertical crosses, and the plasma-less model by a dashed line.

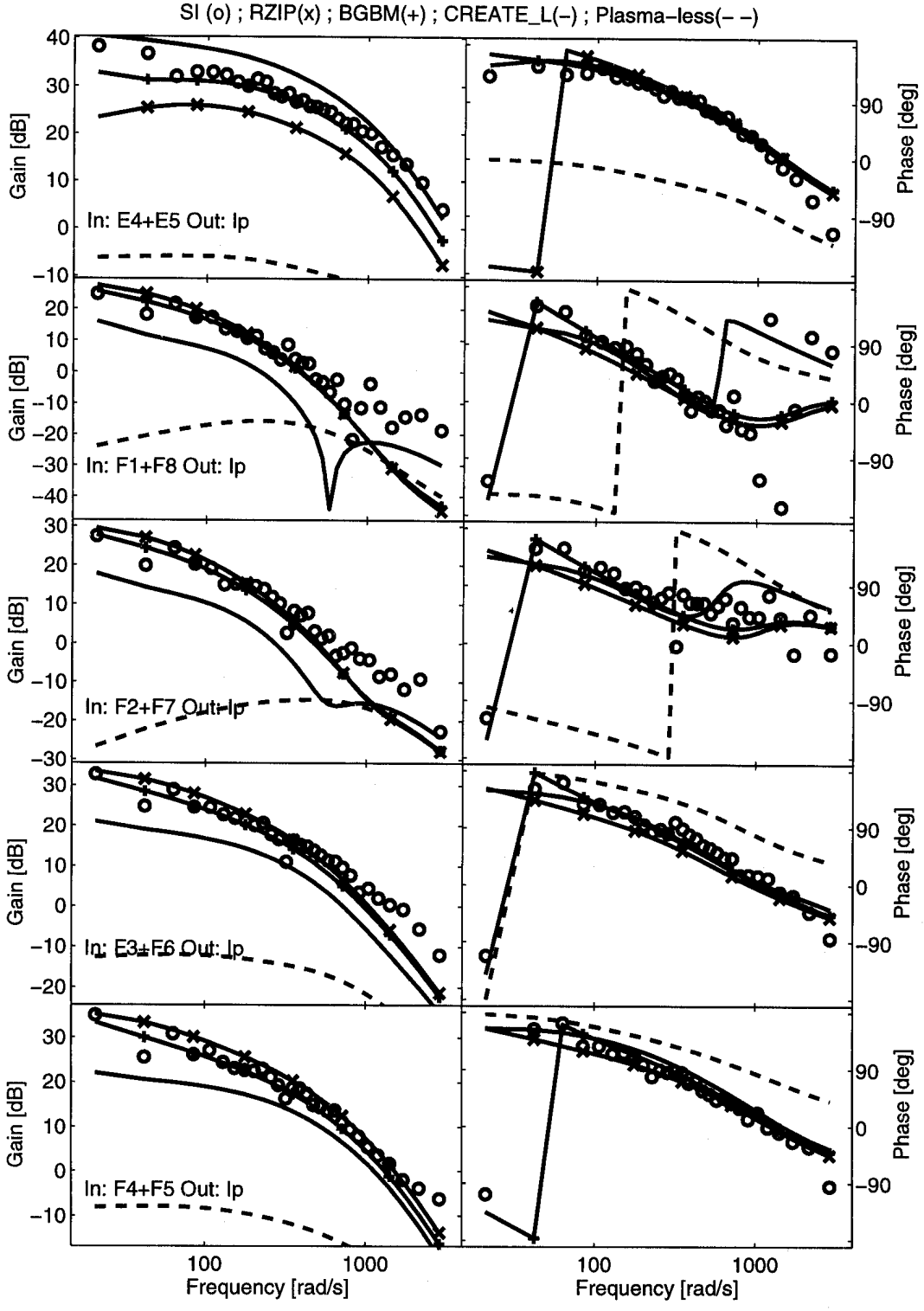

FIG. A10. Frequency response of I_p to symmetric stimulation. The system identified estimates are indicated by circles, the CREATE-L response is indicated by a solid line, RZIP by a line with diagonal crosses, the BGBM response by a line with vertical crosses, and the plasma-less model by a dashed line.

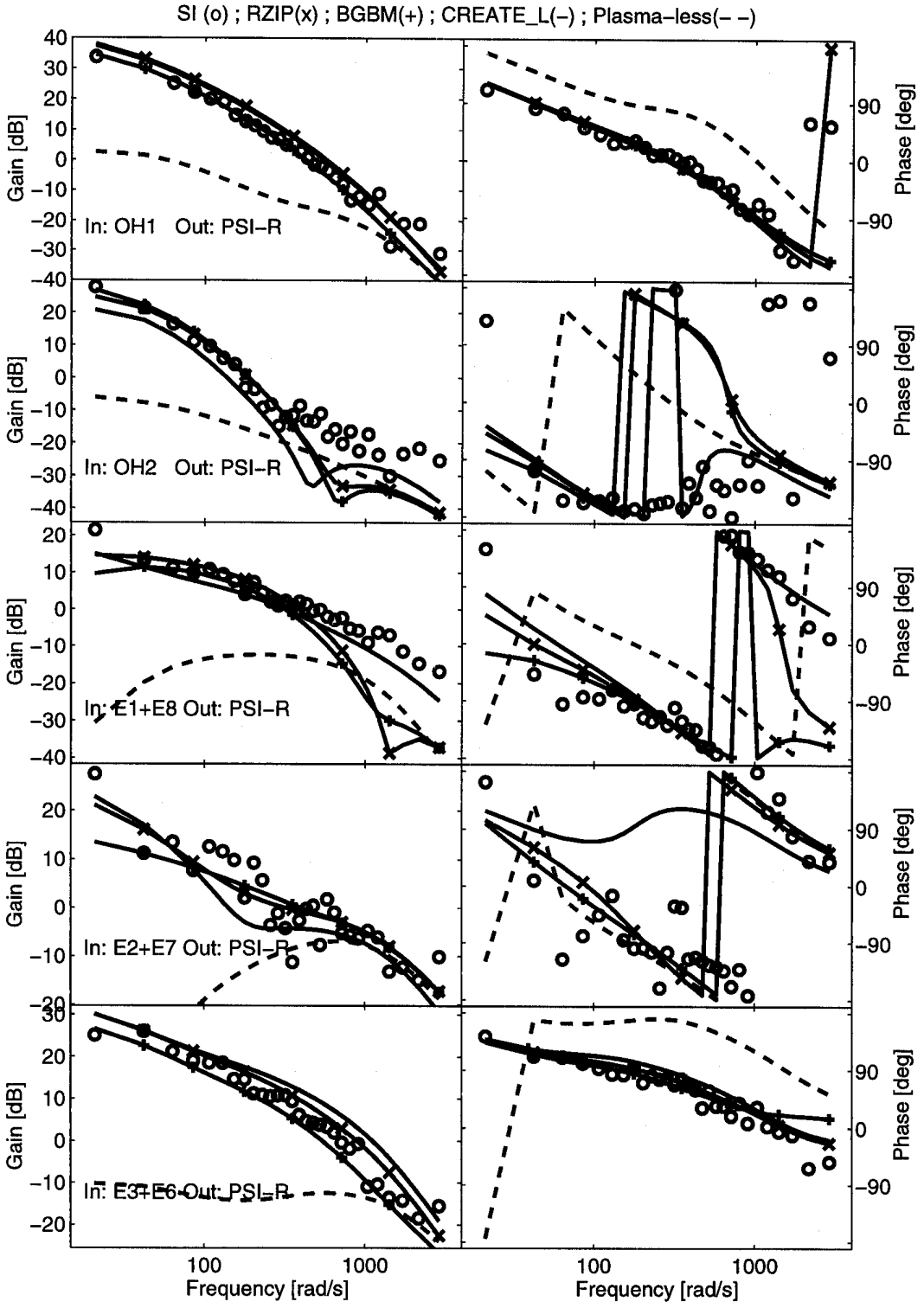

FIG. A11. Frequency response of Ψ_R to symmetric stimulation. The system identified estimates are indicated by circles, the CREATE-L response is indicated by a solid line, RZIP by a line with diagonal crosses, the BGBM response by a line with vertical crosses, and the plasma-less model by a dashed line.

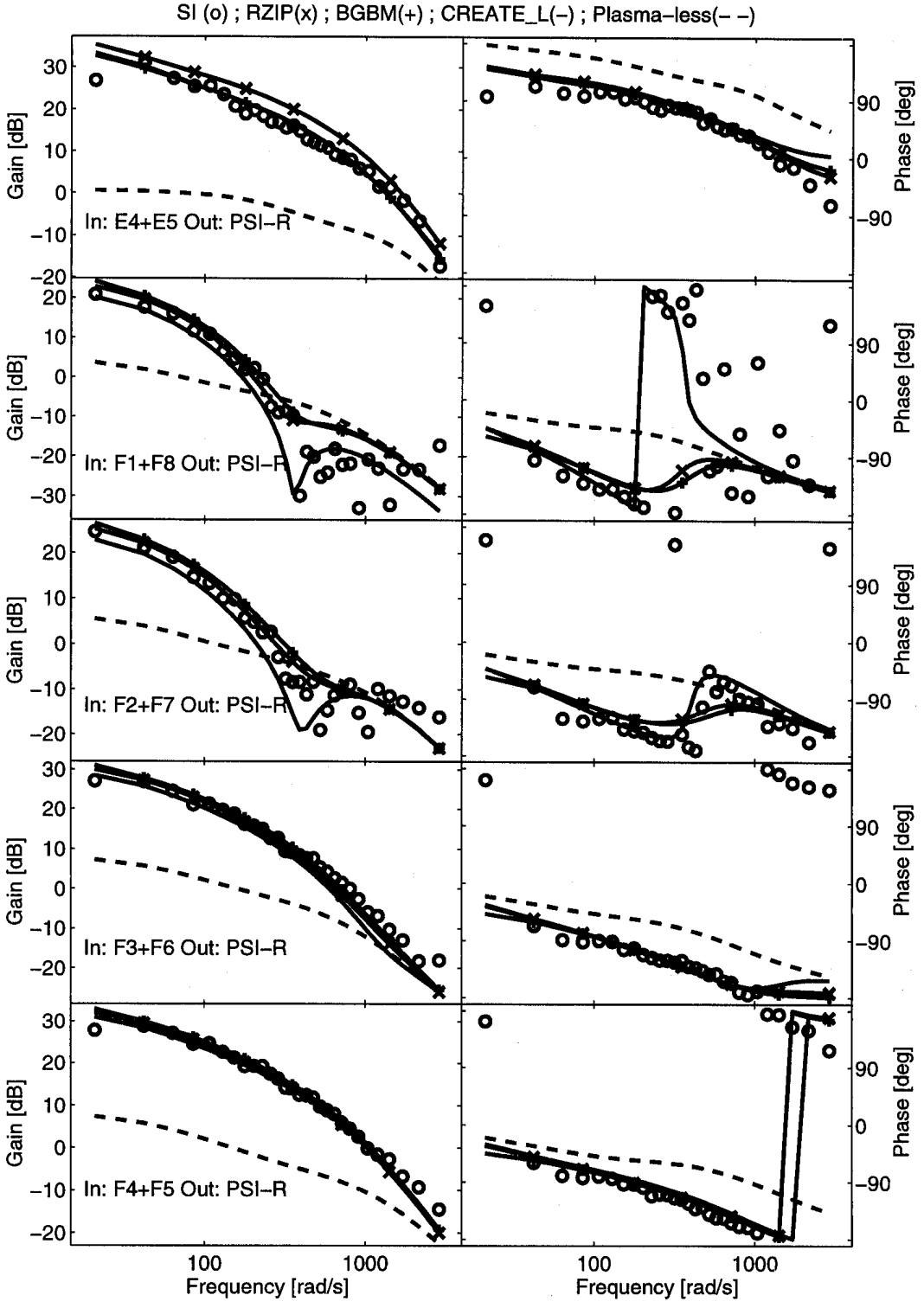

FIG. A12. Frequency response of Ψ_R to symmetric stimulation. The system identified estimates are indicated by circles, the CREATE-L response is indicated by a solid line, RZIP by a line with diagonal crosses, the BGBM response by a line with vertical crosses, and the plasma-less model by a dashed line.